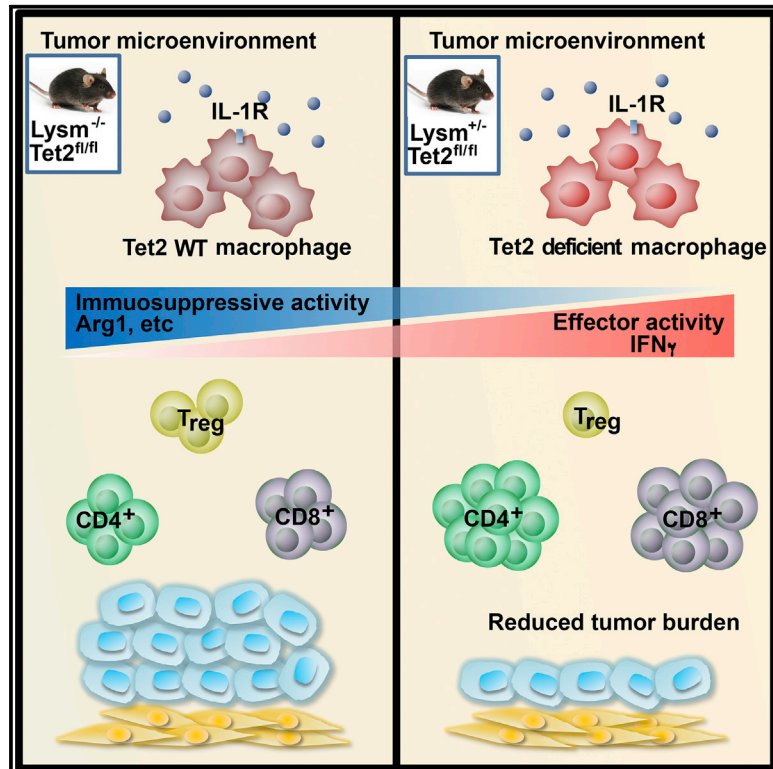


Immunity

The DNA Methylcytosine Dioxygenase Tet2 Sustains Immunosuppressive Function of Tumor-Infiltrating Myeloid Cells to Promote Melanoma Progression

Graphical Abstract



Authors

Wen Pan, Shu Zhu, Kun Qu, ..., Marcus Bosenberg, Richard A. Flavell, Jun Lu

Correspondence

jun.lu@yale.edu

In Brief

The DNA methylcytosine dioxygenase Tet2 functions as a tumor suppressor in multiple contexts, including hematopoietic malignancies. Pan et al. now reveal a tumor-promoting role for Tet2, whereby Tet2 functions to sustain an immunosuppressive program in myeloid cells that in turn dampens the anti-tumor T cell response.

Highlights

- Deletion of *Tet2* in myeloid cells reduces melanoma tumor burden
- *Tet2* expression is induced via the IL-1R-MyD88 axis in tumor-associated macrophages
- Tet2 maintains myeloid immunosuppressive function and the associated genetic program
- Myeloid-specific *Tet2* deletion results in higher numbers of tumor-infiltrating T cells



The DNA Methylcytosine Dioxygenase Tet2 Sustains Immunosuppressive Function of Tumor-Infiltrating Myeloid Cells to Promote Melanoma Progression

Wen Pan,^{1,2} Shu Zhu,^{3,4,5} Kun Qu,⁵ Katrina Meeth,^{6,7} Jijun Cheng,^{1,2} Kaixin He,^{4,5} Hongdi Ma,^{4,5} Yan Liao,⁸ Xizhi Wen,⁹ Christine Roden,^{1,2} Zuzana Tobiasova,³ Zheng Wei,³ Jun Zhao,³ Jun Liu,^{1,2} Ji Zheng,^{1,2,10} Bo Guo,^{1,11} Sajid A. Khan,¹² Marcus Bosenberg,^{6,7} Richard A. Flavell,³ and Jun Lu^{1,2,13,*}

¹Department of Genetics, Yale University School of Medicine, New Haven, CT 06520, USA

²Yale Stem Cell Center, Yale Cancer Center, Yale Cooperative Center of Excellence in Hematology, Yale University, New Haven, CT 06520, USA

³Department of Immunobiology, Yale University School of Medicine, New Haven, CT 06520, USA

⁴Institute of Immunology, University of Science and Technology of China, Hefei 230027, China

⁵CAS Key Laboratory of Innate Immunity and Chronic Disease, School of Life Sciences and Medical Center, University of Science and Technology of China, Hefei 230027, China

⁶Department of Pathology, Yale University School of Medicine, New Haven, CT 06519, USA

⁷Department of Dermatology, Yale University School of Medicine, New Haven, CT 06519, USA

⁸Center for Stem Cell Biology and Tissue Engineering, Key Laboratory for Stem Cells and Tissue Engineering, Ministry of Education, Sun Yat-Sen University, Guangzhou 510060, China

⁹Biotherapy Center, Sun Yat-Sen University Cancer Center; State Key Laboratory of Oncology in South China; Collaborative Innovation Center for Cancer Medicine, Guangzhou 510060, China

¹⁰Department of Urology, Southwest Hospital, Third Military Medical University, Chongqing 400038, China

¹¹General Hospital of People's Liberation Army, Beijing, China

¹²Department of Surgery, Yale University School of Medicine, New Haven, CT 06519, USA

¹³Lead Contact

*Correspondence: jun.lu@yale.edu

<http://dx.doi.org/10.1016/j.immuni.2017.07.020>

SUMMARY

Ten-Eleven-Translocation-2 (*Tet2*) is a DNA methylcytosine dioxygenase that functions as a tumor suppressor in hematopoietic malignancies. We examined the role of *Tet2* in tumor-tissue myeloid cells and found that *Tet2* sustains the immunosuppressive function of these cells. We found that *Tet2* expression is increased in intratumoral myeloid cells both in mouse models of melanoma and in melanoma patients and that this increased expression is dependent on an IL-1R-MyD88 pathway. Ablation of *Tet2* in myeloid cells suppressed melanoma growth *in vivo* and shifted the immunosuppressive gene expression program in tumor-associated macrophages to a proinflammatory one, with a concomitant reduction of the immunosuppressive function. This resulted in increased numbers of effector T cells in the tumor, and T cell depletion abolished the reduced tumor growth observed upon myeloid-specific deletion of *Tet2*. Our findings reveal a non-cell-intrinsic, tumor-promoting function for *Tet2* and suggest that *Tet2* may present a therapeutic target for the treatment of non-hematologic malignancies.

INTRODUCTION

Tumor-tissue myeloid cells have important roles in anti-tumor immunity and tumor progression. Monocytes, macrophages, and granulocytes are actively recruited to tumors where they interact with the tumor microenvironment, often to accelerate tumor progression. Tumor-associated macrophages (TAMs) and myeloid-derived suppressor cells (MDSCs) are often regarded as having immunosuppressive functions that promote tumor growth, in part by suppressing adaptive immune responses to tumor cells (Marvel and Gabrilovich, 2015; Ostuni et al., 2015; Qian and Pollard, 2010; Yadav and Delamarre, 2016). TAMs are phenotypically and functionally distinct from tissue-resident macrophages (Franklin et al., 2014). The tumor microenvironment acts on the gene expression program of TAMs to establish and maintain immunosuppressive functions (Amit et al., 2016; Church and Galon, 2015; Colegio et al., 2014; Noy and Pollard, 2014). Factors responsible for the establishment and maintenance of TAM functions are beginning to emerge (Colegio et al., 2014). In particular, proteins associated with the regulation of DNA methylation, and thereby gene expression, present interesting candidates.

Ten-Eleven-Translocation-2 (*Tet2*) is an important tumor suppressor within the hematopoietic system. Loss-of-function mutations in *TET2*, such as mutations resulting in reading-frameshifts and early stop codons, are frequently found in myeloid malignancies (Delhommeau et al., 2009; Figueroa et al., 2010; Ko et al., 2010; Langemeijer et al., 2009). Deletion

of *Tet2* in hematopoietic stem cells (HSCs) leads to increased self-renewal of HSCs and the expansion of the myeloid compartment, particularly the myelomonocytic lineage (Ko et al., 2011; Li et al., 2011; Moran-Crusio et al., 2011; Quivoron et al., 2011), further supporting a tumor-suppressive role for *Tet2*. *Tet2*, together with *Tet1* and *Tet3*, form the Tet family, which biochemically catalyzes 5-methylcytosine (5mC) conversion to 5-hydroxymethylcytosine (5hmC) and its derivatives to mediate DNA demethylation (He et al., 2011; Huang and Rao, 2014; Ito et al., 2011; Tahiliani et al., 2009; Wu and Zhang, 2011). Recent studies have also revealed non-catalytic functions of *Tet2* (Chen et al., 2013; Zhang et al., 2015), underscoring diverse mechanisms by which *Tet2* regulates gene expression.

Although the function of *Tet2* as a hematopoietic tumor suppressor is well established, it is unclear whether *Tet2* activity within hematopoietic cells could impact solid tumors. In particular, the expansion of myelomonocytic lineages upon *Tet2* deletion in HSCs raises the question of whether distinct functions of *Tet2* may exist in these cells. Furthermore, recent findings of somatic *TET2* mutations in peripheral blood cells, present in both healthy human individuals and solid cancer patients (Busque et al., 2012; Genovese et al., 2014; Jaiswal et al., 2014; Xie et al., 2014), raise the possibility that *TET2* mutant myeloid cells may be “genetically reprogrammed” to elicit altered functions in solid cancer. Roles for *Tet2* in T cells (Ichihama et al., 2015; Tsagaratou et al., 2014; Yang et al., 2015) and dendritic cells in response to pathogens (Zhang et al., 2015) have been recently described. Whether *Tet2* could impact gene expression and thereby function of TAMs and how *Tet2* might be regulated by the tumor environment remains to be investigated.

Successes of immune-checkpoint inhibitors in melanoma patients highlight the potential of immune cells in regulating melanoma biology (Bhatia and Thompson, 2014; Callahan, 2016). Human melanomas harbor activation mutations in *BRAF*^{V600E} in ~65% of cases (Chin, 2003; Davies et al., 2002), which often co-occur with loss-of-function mutations in tumor suppressors such as *PTEN* and *CDKN2A*. A mouse model of melanoma bearing the *Braf*^{V600E} and *Pten*^{null} mutations recapitulates key features of human melanoma (Dankort et al., 2009). Treatment of these mice with an inhibitor of the macrophage colony-stimulating factor receptor (*Csf1r*, important for macrophage differentiation, proliferation, and survival) delayed tumorigenesis, suggesting the importance of TAMs in promoting tumor development in this model (Ngiow et al., 2015).

Here we explored the impact of myeloid-specific deletion of *Tet2* on tumor growth using two murine melanoma models. Contrary to the recognized role of *Tet2* as a tumor suppressor, we found that *Tet2* maintains the immunosuppressive functions of tumor-tissue macrophages to promote tumor growth. *Tet2* expression in TAMs was regulated via an interleukin-1 receptor (IL-1R)-Myd88 pathway, and deletion of *Tet2* resulted in changes in gene expression and associated functional polarization of TAMs. Thus, *Tet2*, a protein regulating the DNA methylation landscape, mediates myeloid immunosuppression and melanoma tumor progression.

RESULTS

Increased Expression of *Tet2* in TAMs and MDSCs during Melanoma Progression

As a main model in our study, we used the YUMM1.7 murine melanoma cell line, which was derived from the *Braf*^{V600E}*Pten*^{-/-}*Cdkn2a*^{-/-} mouse model (Dankort et al., 2009). YUMM1.7 robustly gives rise to melanoma in syngeneic wild-type host mice with a substantial contribution of TAMs to tumor mass (Ho et al., 2015; Meeth et al., 2016), similar to what is often observed in human melanoma.

We first evaluated the RNA expression levels of Tet family members in myeloid cells after injecting YUMM1.7 cells subcutaneously into wild-type mice (Figure 1A). We found that TAMs isolated from tumor tissue had significantly higher *Tet2* mRNA expression than macrophages isolated from peritoneum or bone marrow of control tumor-free mice (Figure 1B). In contrast, *Tet3* mRNA expression levels were similar between these macrophage populations (Figure 1B), whereas *Tet1* transcripts were barely detectable. We next harvested TAMs at two different time points during tumor progression (early and late stages) and determined that the amounts of *Tet2* transcripts in TAMs increased during melanoma progression, whereas no change in *Tet3* expression was observed (Figure 1C). Consistent with the increase of *Tet2* mRNA expression, global 5hmC levels in TAM genomic DNA were increased by ~2-fold during melanoma progression (Figure 1D). To further characterize *Tet2* gene expression, we examined *Tet2* RNA levels in TAMs, intratumoral MDSCs (CD11b⁺Gr1⁺), as well as splenic macrophages, splenic monocytic MDSCs (M-MDSCs; CD11b⁺Ly6C^{hi}Ly6G⁻), and splenic granulocytic MDSCs (G-MDSC; CD11b⁺Ly6C^{lo}Ly6G⁺) from tumor-bearing mice (see Figure S1A for sorting scheme). Overall, intratumoral myeloid cells had ~2-fold higher *Tet2* mRNA levels than the corresponding splenic populations from tumor-bearing mice, which in turn were ~2-fold higher than corresponding splenic populations from non-tumor-bearing mice (Figure 1E). We also observed that granulocytic populations had 2- to 3-fold lower *Tet2* mRNA amounts than macrophage and monocytic populations from the same tissue, while *Tet3* RNA levels were similar across all these subsets (Figure 1E). Similar results were observed when another melanoma model was used, induced by injecting B16-OVA cells (Figures S1B and S1C). To determine whether increased *Tet2* expression in intratumoral myeloid cells is also seen in human melanoma, we isolated intratumoral and circulating CD11b⁺ myeloid cells from six melanoma patients. Intratumoral myeloid cells exhibited higher amounts of *Tet2* mRNA than peripheral myeloid cells, whereas no appreciable difference was noted in *Tet3* RNA amounts (Figures 1F). Taken together, the data above indicate that *Tet2* expression is increased in TAMs and MDSCs during tumor progression, suggesting regulation by the tumor microenvironment.

Myeloid-Specific Deletion of *Tet2* Suppresses Melanoma Growth

We next asked whether *Tet2* in myeloid cells regulates tumor progression. We crossed *Tet2*^{fl/fl} mice with LysM-cre mice to ablate *Tet2* in the myeloid compartment, including macrophages (referred to as “Mye-*Tet2* null”). Macrophages from

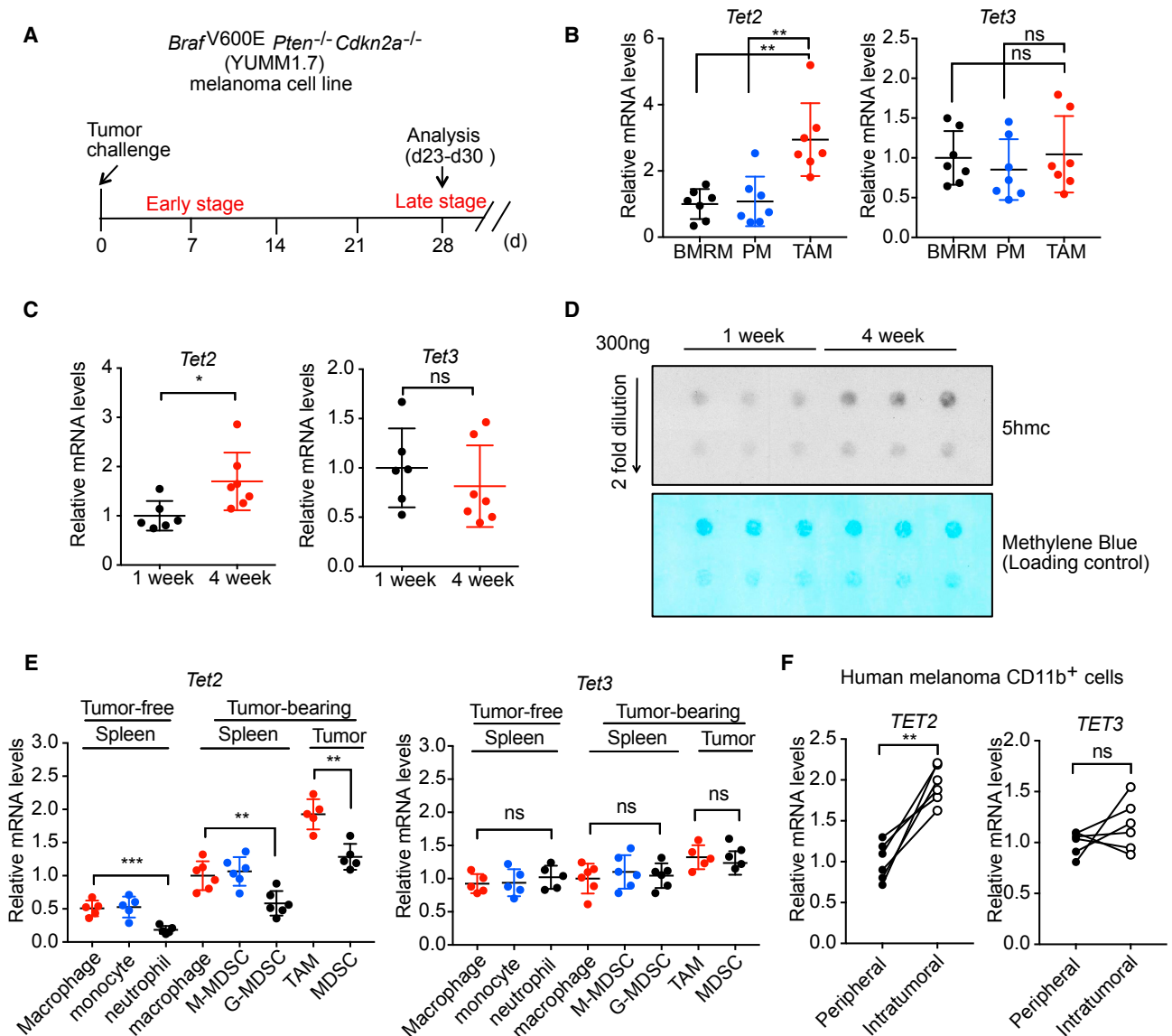


Figure 1. Increased Amounts of *Tet2* Transcripts in TAMs and MDSCs during Melanoma Progression

(A) Schematic illustration of the syngeneic tumor model in which *Braf*^{V600E}*Pten*^{-/-}*Cdkn2a*^{-/-} (YUMM1.7) melanoma cells were injected subcutaneously. Tumor-associated macrophages (TAMs) were harvested at 1 and 4 weeks.

(B) *Tet2* and *Tet3* transcript amounts were determined in peritoneal macrophages (PM) and bone marrow-resident macrophages (BMRMs) from tumor-free mice and TAMs (4 weeks after tumor cell injection) from tumor-bearing wild-type (WT) mice, using qRT-PCR. *n* = 7. Normalized RNA expression is shown with each dot reflecting one mouse.

(C) TAMs were harvested from WT mice at 1 week (*n* = 6) and 4 weeks (*n* = 7) after tumor cell injection. *Tet2* and *Tet3* transcript amounts were determined by qRT-PCR. Normalized RNA expression is shown with each dot reflecting one mouse.

(D) TAMs were harvested from WT mice at the indicated time points after tumor cell injection. 5hmC levels in genomic DNA were determined by dot blot analysis, with methylene blue staining used as a loading control.

(E) *Tet2* and *Tet3* transcript levels were determined in TAMs and MDSCs purified from tumor mass, splenic macrophages, monocytic MDSCs (M-MDSCs), and granulocytic MDSCs (G-MDSCs) purified from tumor-bearing WT mice, as well as splenic macrophages, monocytes, and granulocytes purified from WT mice without tumor.

(F) *Tet2* and *Tet3* transcript levels were determined in peripheral and intratumoral CD11b⁺ myeloid cells isolated from six human melanoma patients. Each line connects samples from the same patient.

For all panels, **p* < 0.05; ***p* < 0.01; ns, not significant. Data are representative of three (B–E) or two (D) independent experiments. Please also see Figure S1.

Mye-Tet2-null mice had ~80% reduction in Tet2 expression, which is consistent with the reported ~70%–80% deletion efficiency in the LysM-cre model (Abram et al., 2014; Ye et al.,

2003). We first determined that Mye-Tet2-null mice did not affect steady-state myeloid cell lineage distribution. Indeed, similar numbers and percentages of myeloid populations, including

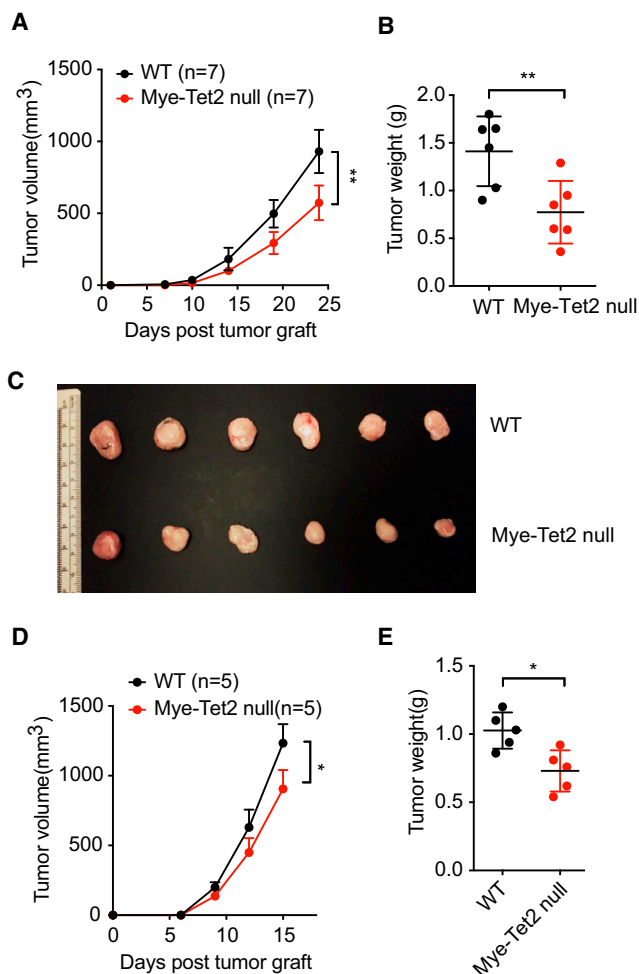


Figure 2. Myeloid-Specific Deletion of *Tet2* Inhibits Melanoma Growth

(A–C) YUMM1.7 melanoma cells were injected into WT and Mye-Tet2-null mice.

(A) Mean tumor volume in WT and Mye-Tet2-null mice. $n = 7$.

(B) Tumor weights 4 weeks after tumor cell injection. $n = 6$.

(C) Pictures of tumors for (B).

(D and E) B16-OVA melanoma cells were injected into WT and Mye-Tet2-null mice.

(D) Mean tumor volume in WT and Mye-Tet2-null mice. $n = 5$.

(E) Tumor weights at the endpoint for (D).

For all panels, $*p < 0.05$; $**p < 0.01$; ns, not significant. Data are representative of three (A–C) or two (D, E) independent experiments.

macrophage and monocytic cells, were observed in spleen or bone marrow from 6- to 8-week-old *LysMcre*^{+/^{wt}}*Tet2*^{fl/fl} mice, compared to wild-type control (WT, *LysMcre*^{wt/wt}*Tet2*^{fl/fl}) mice (Figures S1D and S1E). We next asked whether myeloid-specific deletion of *Tet2* affected melanoma growth. We injected YUMM1.7 melanoma cells into syngeneic Mye-Tet2-null or WT host mice. Mye-Tet2-null mice exhibited significantly slower tumor growth (Figure 2A) and bore substantially smaller tumors than WT mice (Figures 2B and 2C). Similar results were observed when the B16-OVA melanoma model was used (Figures 2D and 2E). Taken together, the data above indicate that deletion of *Tet2* in myeloid cells leads to the suppression of tumor growth.

***Tet2* Expression Is Increased by IL-1 Receptor Signaling and Dependent on the MyD88 Pathway**

The increase of *Tet2* mRNA amounts in TAMs during tumor progression suggests that *Tet2* is regulated by the tumor microenvironment. To investigate possible pathways controlling *Tet2* expression, we hypothesized that IL-1 receptor signaling may regulate *Tet2* expression. Several previous studies have demonstrated IL-1 cytokines as important factors in tumor regulation (Carmi et al., 2009; Cataisson et al., 2012; Lewis et al., 2006; Voronov et al., 2014) and that IL-1 cytokines are elevated in primary melanoma tissues (Voronov et al., 2003). We first performed a series of *in vitro* assays on bone marrow-derived macrophages (BMDMs) and found that IL-1R signaling strongly increases *Tet2* expression. Treatment of BMDMs with IL-1 β markedly increased *Tet2* RNA and *Tet2* protein levels in BMDM cells within hours, while *Tet3* mRNA amounts were not changed (Figures 3A and 3B). Consistent with the increase of *Tet2* mRNA, IL-1 β significantly increased global 5hmC levels in the macrophage genome by ~ 2 -fold within 9 hr (Figure 3C). These data indicate that an IL-1R ligand is sufficient to dynamically increase *Tet2* expression and modulate 5hmC levels in the genome. To determine whether IL-1R signaling is required for sustaining elevated *Tet2* expression in TAMs, we injected YUMM1.7 melanoma cells into *Il1r1*^{-/-} or WT littermate control mice and harvested TAMs from the resultant tumors. Indeed, *Tet2* transcripts, as well as those of the previously established IL-1R downstream genes *Vegfa* and *Mmp9*, were significantly reduced in *Il1r1*^{-/-} TAMs (Figure 3D). As negative controls, the mRNA levels of *Irfb* were unchanged (Figure 3D). We also observed that tumor burden was largely reduced in *Il1r1*^{-/-} mice compared to WT mice (Figure S2A). To determine the effect of acute loss of IL-1R signaling on *Tet2* expression in TAMs and on tumor progression, we established tumor development in WT mice and acutely blocked IL-1R signaling afterward (from day 9 after tumor cell injection) by administering an IL-1R antagonist, IL-1Ra, *in vivo* (Figure 3E). IL-1Ra treatment led to a gradual reduction in tumor size (Figure 3F) and reduced *Vegfa* and *Mmp9* expression in TAMs, both at an early time point before significant tumor size reduction was observed (day 12) and at a later time point when tumor size reduction became obvious (day 18) (Figure 3G). At both time points, we observed significant reductions in *Tet2* RNA amounts in TAMs (Figure 3G). These data support that *Tet2* expression in TAMs is positively regulated by IL-1R signaling within the tumor microenvironment.

MyD88 is an important adaptor protein in the IL-1R-signaling pathway (Muzio et al., 1997; Wesche et al., 1997). To determine the function of MyD88 in regulating *Tet2* expression, we performed IL-1 β treatment on BMDMs derived from WT or *Myd88*^{-/-} mice. In *Myd88*^{-/-} cells, we observed that the IL-1 β -induced increase of *Tet2* expression was abolished (Figure 3H), indicating that an IL-1R-MyD88 pathway regulates *Tet2* expression *in vitro*. To determine the function of MyD88 in *Tet2* regulation *in vivo*, we injected YUMM1.7 melanoma cells into WT or *Myd88*^{-/-} mice. Consistent with the *in vitro* data, *Tet2* mRNA levels, as well as those of the canonical MyD88 downstream gene *Il12b*, were reduced in TAMs in *Myd88*^{-/-} mice (Figure 3I), while the levels of *Irfb* were unchanged (Figure 3I). These results support a role for MyD88 in controlling *Tet2* expression in TAMs.

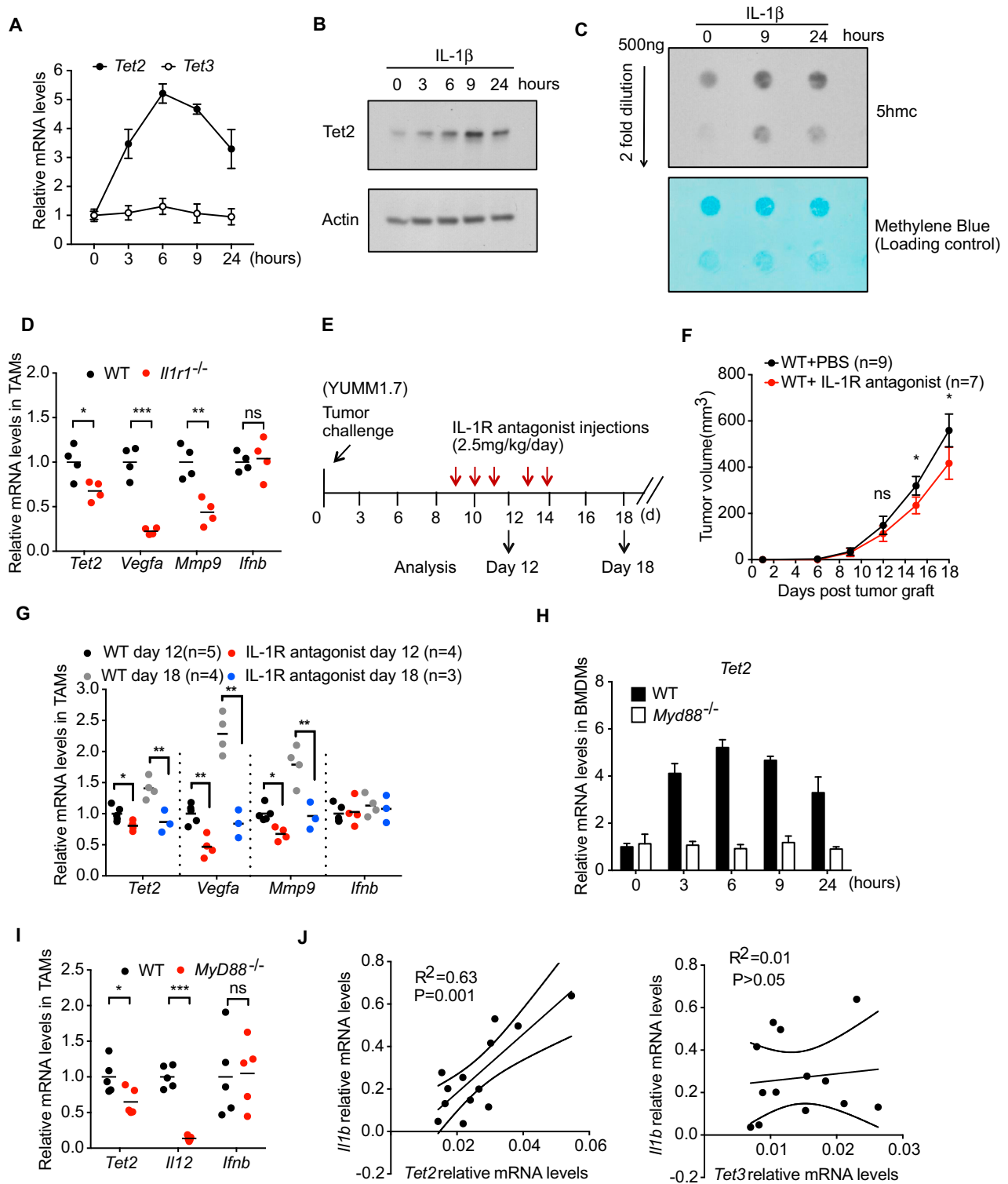


Figure 3. *Tet2* Transcripts Are Increased by IL-1 Receptor Signaling and Dependent on the MyD88 Pathway

(A–C) Bone marrow-derived macrophages (BMDMs) were treated with 100 ng/mL IL-1 β for the indicated hours.

(A) *Tet2* and *Tet3* transcript levels were determined by qRT-PCR.

(B) Representative western blot of *Tet2* protein levels, with beta actin as a loading control.

(C) Representative dot blot of 5hmC levels in genomic DNA for the indicated time points. Methylene blue staining was used as a loading control.

(legend continued on next page)

IL-1R signaling has been shown to increase *I11b* gene expression (Cataisson et al., 2012). Consistent with an IL-1R-MyD88 pathway regulating *Tet2* expression, we observed a significant correlation between *Tet2* and *I11b* mRNA amounts when examining TAMs harvested from murine melanomas, but not between *Tet3* and *I11b* RNA levels (Figure 3J). Interestingly, when examining peripheral and intratumoral myeloid cells from human melanoma patients, we also observed a significant correlation between *TET2* and *IL1B* transcripts, as well as between those of *TET2* and *IL1A* (Figures S2B and S2C), suggesting that this regulatory pathway operates similarly in human cells. Taken together, the data above support an IL-1R-MyD88-Tet2 pathway in the tumor microenvironment regulating melanoma progression *in vivo*.

Tet2 Sustains the Expression of Immunosuppressive Genes in TAMs

To understand how Tet2 in myeloid cells regulates melanoma progression, we performed RNA-seq analysis on TAMs isolated from tumor-bearing mice of WT and Mye-Tet2-null genotypes. We observed that genes with reduced mRNA expression in Mye-Tet2-null TAMs were enriched for signatures of M2 immunosuppressive macrophages, whereas genes with increased expression in Mye-Tet2-null TAMs were enriched for signatures of M1 proinflammatory macrophages (Figure 4A). We further validated the reduced mRNA expression of a number of genes with immunosuppressive functions, including *Arg1*, *Mgl2*, and *I14* (Figure 4B; Biswas et al., 2008; Rawal et al., 2011; Sharda et al., 2011). At the same time, the mRNA amounts of a number of pro-inflammatory cytokines were increased, including *I16*, *I112b*, and *Tnfa* (Figure 4B). These data indicate that deletion of *Tet2* shifted the balance between immunosuppressive and proinflammatory polarization of TAMs. The effect of *Tet2* deletion on immunosuppressive gene expression was similarly observed when WT or Tet2-null BMDMs were polarized *in vitro* with IL-4 (Figure S3A). The mRNA expression levels of several immunosuppressive genes such as *Arg1* and *Mgl2* were reduced in both Mye-Tet2-null TAMs and IL-4 polarized Tet2-null BMDMs (Figures 4B and S3B). We further evaluated the protein activity of *Arg1* and confirmed decreased *Arg1* activity in Tet2-null TAMs (Figure 4C) and BMDMs (Figure S3C). These data establish that Tet2 is required to maintain the expression of multiple immunosuppressive genes in TAMs.

We next asked whether the reduced expression of immunosuppressive genes can be explained by changes in local 5hmC

alterations. Due to the difficulty of obtaining large numbers of TAMs, we performed genome-wide 5hmC DNA immunoprecipitation (5hmC-DIP) mapping in naive (M0) and polarized (M2) BMDM cells from WT and Tet2-null mice. Overall, 5hmC levels around protein-coding genes were mildly decreased in Tet2-null cells (Figure S3D). Among the genes regulated by Tet2, *Arg1* showed putative differential 5hmC peaks in gene-proximal regions (Figure S3E). We observed that the upstream region of *Arg1* contained a consistently reduced 5hmC peak in Tet2-null cells. The peak region was located close to a known enhancer region of *Arg1* (Figure S3F; Sharda et al., 2011). Using DNA immunoprecipitation (DIP)-qPCR, we confirmed the decreased 5hmC levels at this region in Tet2-null BMDM cells and observed a concomitant increase in 5mC levels (Figure S3G). Similar results were also observed in Mye-Tet2-null TAMs (Figure S3H). These data suggest that Tet2 is required to maintain a low 5mC level at the *Arg1* gene locus by increasing 5hmC levels, implying regulation of the gene by DNA demethylation. However, other immunosuppression-related genes, such as *Mgl2*, *Klf4*, and *Irf4*, did not show major changes in 5hmC levels in gene-proximal regions. Whether these genes could be regulated through a 5hmC-independent mechanism or through 5hmC-dependent distal enhancers requires future analysis. Collectively, our data support that Tet2 maintains the expression of immunosuppressive genes in TAMs, likely through multiple mechanisms.

Reduced Immunosuppressive Functions of Tet2-Null Myeloid Cells *In Vitro*

Guided by the gene expression analysis, we tested whether Tet2-null TAMs and MDSCs have reduced immunosuppressive function, by an *in vitro* T cell activation assay. Specially, splenic CD4⁺ T cells were stimulated with anti-CD3 and anti-CD28 and T cell activation was determined by CFSE-based dye dilution (Doedens et al., 2010). When co-culturing CD4⁺ T cells with WT TAMs, strong suppression of T cell proliferation was observed (Figures 4D and 4E). In contrast, the suppressive capacity was significantly reduced when Mye-Tet2-null TAMs were used, under two different T cell to TAM ratios (Figures 4D and 4E). Similar results were observed when supernatants from IL-4-polarized WT or Tet2-null BMDMs were assayed (Figures S3I and S3J). Since MDSCs are also known to possess immunosuppressive functions and can regulate tumor development, we also examined intratumoral MDSCs and found that both *Arg1* mRNA amounts and *Arg1* protein activity were

(D) YUMM1.7 melanoma cells were injected into wild-type (WT) or *I11r1*^{-/-} mice. Tumor-associated macrophages (TAMs) were harvested 4 weeks after injection. Transcript levels of *Tet2*, *Vegfa*, *Mmp9*, and *I1fnb* were determined by qRT-PCR, with each dot representing a mouse. n = 4.

(E-G) The effect of acute inhibition of IL-1R signaling by an IL-1R antagonist on *Tet2* transcripts and tumor progression.

(E) Experimental schematics.

(F) Tumor volume.

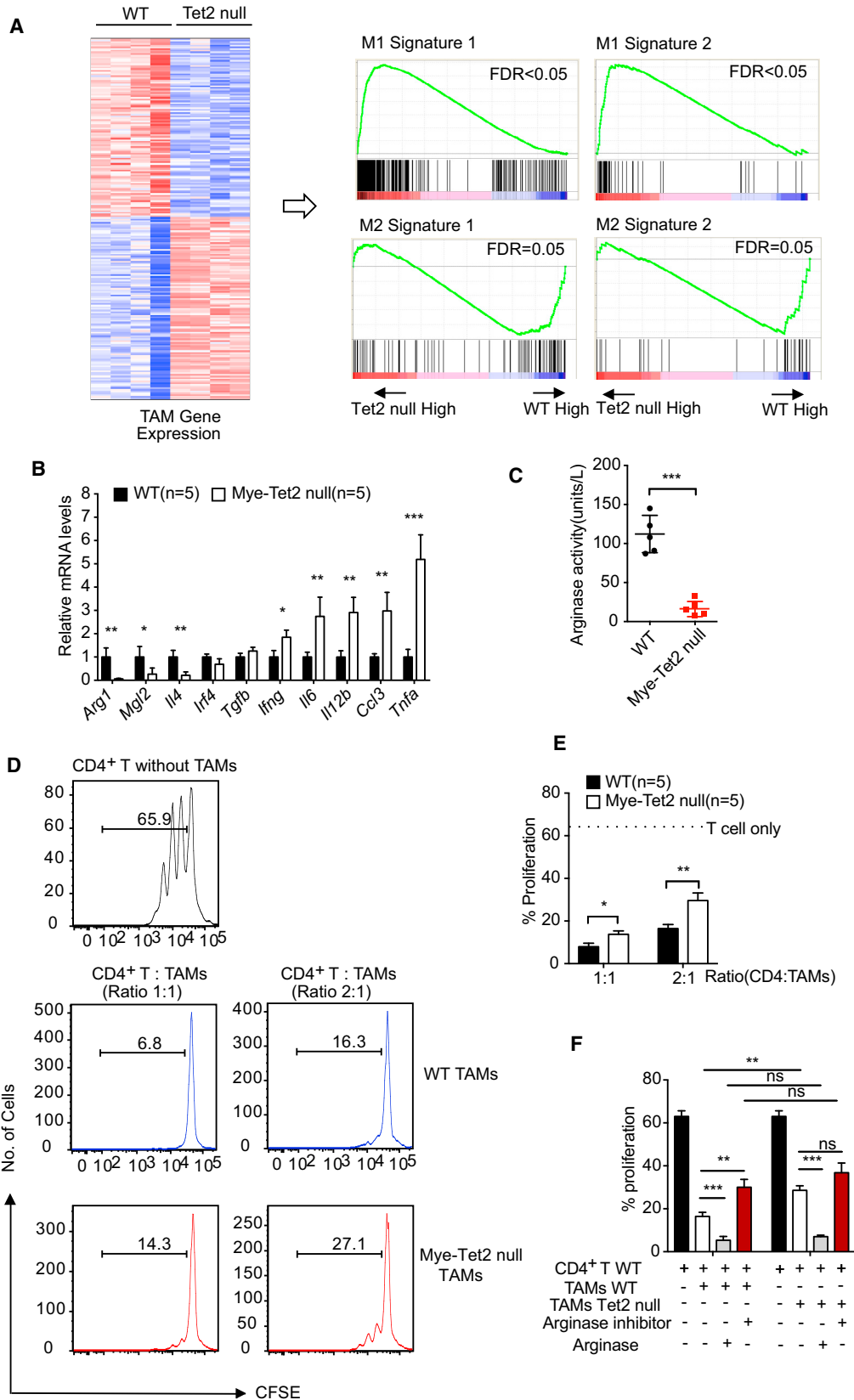
(G) TAMs were harvested at day 12 and day 18. Transcript levels of *Tet2*, *Vegfa*, *Mmp9*, and *I1fnb* were determined by qRT-PCR, with each dot representing a mouse.

(H) WT or *Myd88*^{-/-} BMDMs were treated with 100 ng/mL IL-1β for the indicated hours. *Tet2* transcript levels were determined by qRT-PCR.

(I) YUMM1.7 melanoma cells were injected into wild-type (WT) or *Myd88*^{-/-} mice. TAMs were harvested 4 weeks after injection. Transcript levels of *Tet2*, *I112b*, and *I1fnb* were determined by qRT-PCR, with each dot representing a mouse. n = 5.

(J) Correlation analysis of the transcript levels of *I11b* with those of *Tet2* and *Tet3* were determined in TAMs isolated from week 1 and week 4 YUMM1.7 tumors in WT mice.

For all panels, *p < 0.05; **p < 0.01; ns, not significant. Error bars represent SEM. Data are representative of three independent experiments. Please also see Figure S2.



(legend on next page)

reduced in Tet2-null MDSCs, while reactive oxygen species (ROS) and *iNos*, *Nox2*, *Ncf1*, and *Tgfb* mRNA expression did not show significant changes (Figures S4A–S4C). We next measured the ability of intratumoral MDSCs to suppress T cells. While a decreased immunosuppressive function was observed for Tet2-null MDSCs at a T cell to MDSC ratio of 3:1 (Figures S4D and S4E), significant changes could not be detected when a different ratio was used (Figure S4E), unlike what we observed with TAMs (Figure 4E). These data support a reduction of immunosuppressive functions of Tet2-null TAMs and Tet2-null intratumoral MDSCs, with a stronger alteration in TAMs.

Since *Arg1* gene expression was significantly reduced in Tet2-null TAMs, we asked whether Arg1 is an important mediator of Tet2 function in TAMs. In the TAM and CD4⁺ T cell co-culture, the addition of arginase inhibitor significantly reduced the immunosuppressive activity of WT TAMs, but not that of Mye-Tet2-null TAMs, leading to the abolishment of the difference on T cell suppression by these two groups of cells (Figure 4F). On the other hand, addition of recombinant Arg1 led to an almost complete blockage of T cell proliferation for both WT and Mye-Tet2-null TAMs, again abolishing the difference between these two TAM populations (Figure 4F). These data support that *Arg1* expression plays an important role in mediating the immunosuppressive function of Tet2 in TAMs.

Increased Tumor-Infiltrating T Cells in Mice with Myeloid-Specific Deletion of Tet2

The reduction of the expression of immunosuppressive genes and the reduction of *in vitro* immunosuppressive functions of Mye-Tet2-null TAMs raised the possibility that the intratumoral immune cell repertoire was shifted to favor anti-tumor functions. We thus examined multiple immune subsets (Figure S5A) within the YUMM1.7-initiated tumors developed in WT or Mye-Tet2-null mice. We observed that the percentages of CD45⁺ cells were increased in tumors from Mye-Tet2-null mice (Figure 5A). Within CD45⁺ cells, the percentages of CD3⁺ T cells were significantly increased, whereas those of natural killer (NK) cells, natural killer T (NKT) cells, and macrophages were unchanged, and the percentages of granulocytes were mildly decreased in tumors (Figure 5B). When quantifying by cell numbers per tumor volume, the differences in granulocytes were no longer observed, with a substantial increase of CD3⁺ T cells and mild increases of TAMs, NK cells,

and NKT cells in Mye-Tet2-null tumors (Figure 5B). We further assessed the CD4⁺ and CD8⁺ T cell populations in tumor. Within the T cell compartment, the levels (both percentages within CD45⁺ cells and cell numbers per tumor volume) of both CD4⁺ and CD8⁺ T cells were increased in Mye-Tet2-null tumors, with a stronger elevation observed for CD8⁺ T cells (Figures 5C and 5D). In contrast, the percentages of CD4⁺ or CD8⁺ cells in the spleens of the tumor-bearing mice were not significantly altered in Mye-Tet2-null mice (Figure 5E). Among intratumoral CD4⁺ T cells, the percentages of T helper 1 (Th1) effector T cells were mildly increased whereas those of the immunosuppressive regulatory T (Treg) cells were mildly decreased (Figures 5F and 5J). In contrast, the corresponding populations in spleens were not changed (Figures 5G and 5K). Similar results were observed for CD8⁺ T cells (Figures 5H, 5I, 5L, and 5M). This led to an overall significant elevation of the ratio of CD8⁺ T cells over Treg cells, and a milder increase of the ratio of CD4⁺ T cells over Treg cells (Figure 5N). The increase in the intratumoral T cell populations in Mye-Tet2-null mice, particularly CD8⁺ T cells, could also be observed in the B16-OVA-initiated melanoma, indicating that this effect was not dependent on a specific tumor model (Figures S5B–S5H). Overall, the data here suggest a shift of the intratumoral immune environment to favor anti-tumor activity in Mye-Tet2-null mice.

T Cell Depletion Abolished the Reduced Tumor Growth Observed upon Myeloid-Specific Deletion of Tet2

We reasoned that if increased intratumoral T cells were functionally important for the reduced melanoma growth in Mye-Tet2-null mice, we would expect that depleting T cells could lead to a rescue of tumor size. We tested this possibility by antibody-based depletion of both CD8⁺ and CD4⁺ T cells, given the increase of both cell types observed in YUMM1.7-initiated tumors. After melanoma growth was initiated by injecting WT and Mye-Tet2-null mice with tumor cells, we treated mice with both anti-CD4 and anti-CD8 antibodies from day 7, with one dose per 7 days (Figure 6A). The antibody treatments effectively depleted T cells, as evidenced by the loss of CD4⁺ and CD8⁺ T cell populations in spleen, lymph node, and tumor (Figures 6B). This treatment did not lead to any major noticeable changes in TAMs with regard to both immunostaining and gene expression (Figures S6A and S6B). Similar to the aforementioned phenotypes, mock-treated mice bore tumors with reduce size in Mye-Tet2-null mice compared to WT controls

Figure 4. Tet2 Sustains Immunosuppressive Function and Gene Expression in TAMs

(A) Tumors were initiated by YUMM1.7 cell injection. RNA-seq experiments were performed on TAMs isolated from WT and Mye-Tet2-null mice ~4 weeks after injection. *n* = 4. A heatmap of 214 differentially expressed genes are shown on the left. Right: two independent sets of M1 and M2 macrophage signatures were queried on the TAM gene expression using gene set enrichment analysis (GSEA) to reveal the decrease of M2 signature and the increase of M1 signature in Mye-Tet2-null TAMs. GSEA plots are shown.

(B) qRT-PCR analysis of the mRNA levels of indicated genes in TAMs from WT or Mye-Tet2-null mice. *n* = 5.

(C) TAMs from WT or Mye-Tet2-null mice were analyzed for arginase activity in cell lysates.

(D–F) TAMs purified from WT or Mye-Tet2-null mice were co-cultured with CD4⁺ T cells at the indicated cellular ratios for T cell activation assay. T cell proliferation was quantified by CFSE-labeling and dye dilution for 3 days *in vitro*.

(D) Representative histograms of CFSE signals in the *in vitro* T cell activation assay.

(E) Quantification of CD4⁺ T cell proliferation in (D).

(F) Quantification of CD4⁺ T cell proliferation with recombinant human arginase 1 (1 μg/mL) or arginase inhibitor (100 μM) added into the co-culture medium.

For all panels, **p* < 0.05; ***p* < 0.01; ****p* < 0.001; ns, not significant. Error bars represent SEM. Data for all panels are representative of two or more independent experiments. Please also see Figures S3 and S4.

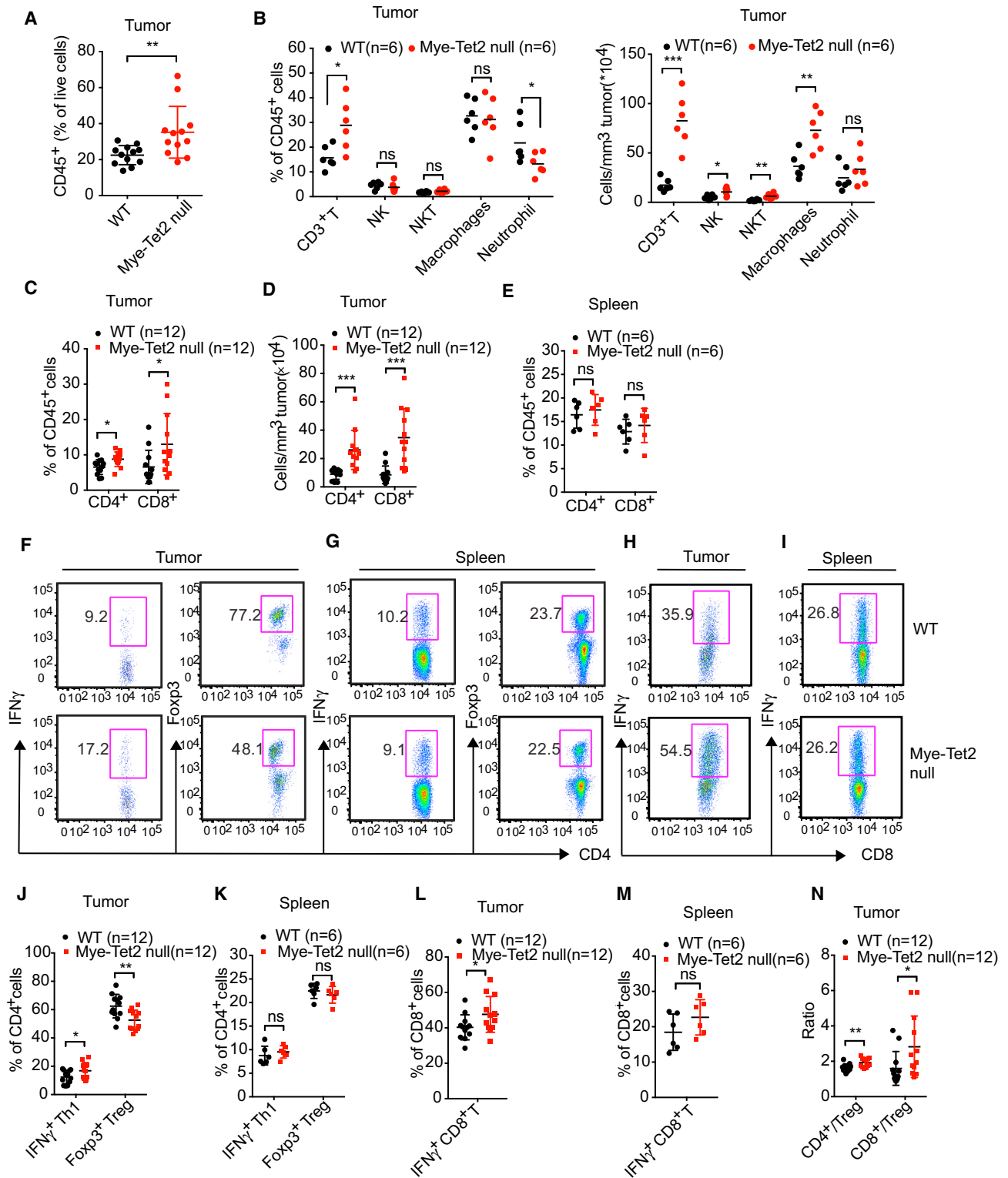


Figure 5. Myeloid-Specific Deletion of *Tet2* Leads to an Increase of Tumor-Infiltrating T Cells

YUMM1.7 melanoma cells were injected into WT or Mye-Tet2-null mice. Tumor-infiltrating immune cells were examined by flow cytometry 4 weeks after injection.

(A) The percentages of tumor-infiltrating CD45⁺ hematopoietic cells within all live cells from the tumor were quantified. Each dot represents one mouse. n = 12.

(legend continued on next page)

(Figure 6C). T cell depletion resulted in a mild increase (1.4-fold) in tumor size in WT mice (Figures 6C and 6E). In contrast, T cell depletion in Mye-Tet2-null mice led to a stronger (>2.2-fold) increase in tumor size. No significant changes were observed when comparing tumor sizes in Mye-Tet2-null mice to those from WT mice upon T cell depletion (Figure 6C). Indeed, statistical analyses confirmed that the reduction of tumor size in Mye-Tet2-null mice were largely abolished upon T cell depletion (Figure 6D) and that T cell depletion had a significantly stronger effect on tumor size in Mye-Tet2-null mice than in WT control mice (Figure 6E). When depleting CD8⁺ and CD4⁺ T cells separately, we observed a stronger effect by CD8⁺ T cell depletion (Figure S6C), consistent with a stronger increase in intratumoral CD8⁺ T cells in the Mye-Tet2-null tumors. Similar effects of CD8⁺ and CD4⁺ T cell depletion were also observed in the B16-OVA-initiated tumor model (Figures S6D and S6E). Taken together, these data indicate that T cell depletion rescued the reduced tumor growth phenotype in Mye-Tet2-null mice.

DISCUSSION

Tet2 is recognized as one of the major tumor suppressors within the hematopoietic system. It is often mutated somatically in hematopoietic cells in healthy individuals, as well as in patients with myeloid malignancies or solid tumors (Busque et al., 2012; Genovese et al., 2014; Jaiswal et al., 2014; Xie et al., 2014). This tumor-suppressive function has been attributed to increased hematopoietic stem and progenitor cells in mice with *Tet2* deletion (Ko et al., 2011; Li et al., 2011; Moran-Crusio et al., 2011; Quivoron et al., 2011). While the expansion of myelomonocytic lineages have been observed when *Tet2* is deleted in murine HSCs, it is unclear whether ablation of *Tet2* in downstream myeloid cells may impact malignant processes. Here, we focus on the myeloid compartment and demonstrate that Tet2 plays a surprising tumor-promoting role in melanoma models by sustaining immunosuppressive functions of intratumoral myeloid cells. Whether this role also applies to other solid cancers awaits future exploration.

Since the cre stain we used cannot genetically distinguish the different myeloid subpopulations, it is likely that both TAMs and MDSCs contribute to the phenotype of reduced tumor growth in mice with myeloid-specific deletion of *Tet2*. Both TAMs and intratumoral MDSCs had higher levels of *Tet2* mRNA

amounts than similar splenic populations of tumor-bearing mice or tumor-free mice. The expression of *Arg1*, the signature gene for TAMs, M2 macrophages, and M-MDSCs, was reduced in TAMs and intratumoral MDSCs. We did not detect a change in ROS level in the intratumoral MDSC population, suggesting that G-MDSCs may be less impacted. On the gene expression level, Mye-Tet2-null TAMs showed a significant increase in the M1 macrophage signature and a concurrent decrease in the M2 macrophage signature. Which of the differentially expressed gene(s) mediates the function of Tet2 on immunosuppression? Our data support that the reduction of *Arg1* is an important event downstream of *Tet2* ablation. These results are consistent with myeloid *Arg1* promoting tumor growth in a lung tumor model *in vivo* (Colegio et al., 2014; Rodriguez et al., 2005) and that *Arg1* catalyzes the degradation of L-arginine from the extracellular environment to decrease antigen-specific T cell proliferation (Pauleau et al., 2004). Our findings on *Arg1*, however, do not exclude the possibility that other Tet2-regulated genes, such as *Mgl2*, also contribute to the phenotype. Similarly, it is also possible that the increase of the M1 macrophage gene expression program in Tet2-null TAMs plays important functional roles.

TAMs are heterogeneous in terms of function and phenotype (Okabe and Medzhitov, 2014). It is highly likely that the different activation states of TAMs reflect responses to dynamic local microenvironmental cues within the tumor (Amit et al., 2016). We examined this topic in our murine tumor models and found an IL-1R-MyD88 pathway enhancing *Tet2* expression both *in vitro* and *in vivo*. Our data on MDSCs and human melanoma specimens suggest that the regulation of Tet2 gene expression by tumor microenvironment could be extended to other myeloid populations and is conserved from mouse to human. IL-1R can be regulated by multiple ligands, including IL-1 β , IL-1 α , and IL-1Ra (Voronov et al., 2014). Our work suggests that cytokines derived from tissue microenvironment can affect the DNA-methylation-related pathway in TAMs and control macrophage function. It is also interesting to note that chronic IL-1 exposure drives HSCs to precociously differentiate toward the myeloid lineage (Pietras et al., 2016). Whether a similar pathway regulates Tet2 during HSC differentiation could be examined in the future.

Our work suggests that the DNA-methylation regulatory pathway in myeloid cells could be further explored to elucidate immune regulation of solid tumors. Other than Tet2, Tet3 and Dnmt3a have been recently reported to modulate gene

(B) For intratumoral cells, the percentages within total CD45⁺ cells (left) or numbers per tumor volume (right) of the indicated immune cell populations were quantified. Each dot represents one mouse. n = 6.

(C and D) Tumor-infiltrating CD4⁺ and CD8⁺ T cells were quantified either as (C) the percentages within total CD45⁺ cells or (D) as absolute numbers per tumor volume. Each dot represents one mouse. n = 12.

(E) The percentages of splenic CD4⁺ and CD8⁺ T cells from tumor-bearing mice were quantified within total CD45⁺ splenocytes. n = 6.

(F–N) Intratumoral T cells or splenic T cells from tumor-bearing mice were further characterized by flow cytometry.

(F and J) Statistical and representative flow cytometry plots showing the percentages of CD4⁺IFN- γ ⁺ Th1 cells and CD4⁺Foxp3⁺ Treg cells within total intratumoral CD4⁺ T cells. Each dot represents one mouse. n = 12.

(G and K) Similar analysis as (F) and (J) was performed on splenic T cells within tumor-bearing mice. n = 6.

(H and L) Statistical and representative flow cytometry plots showing the percentages of CD8⁺IFN- γ ⁺ T cells within total intratumoral CD8⁺ T cells. Each dot represents one mouse. n = 12.

(I and M) Similar analysis as (H) and (L) was performed on splenic T cells within tumor-bearing mice. n = 6.

(N) Ratios of intratumoral CD4⁺ to Treg and CD8⁺ to Treg cells were quantified. Each dot represents one mouse.

For all panels, *p < 0.05; **p < 0.01; ns: not significant. Data are representative of three independent experiments. Please also see Figure S5.

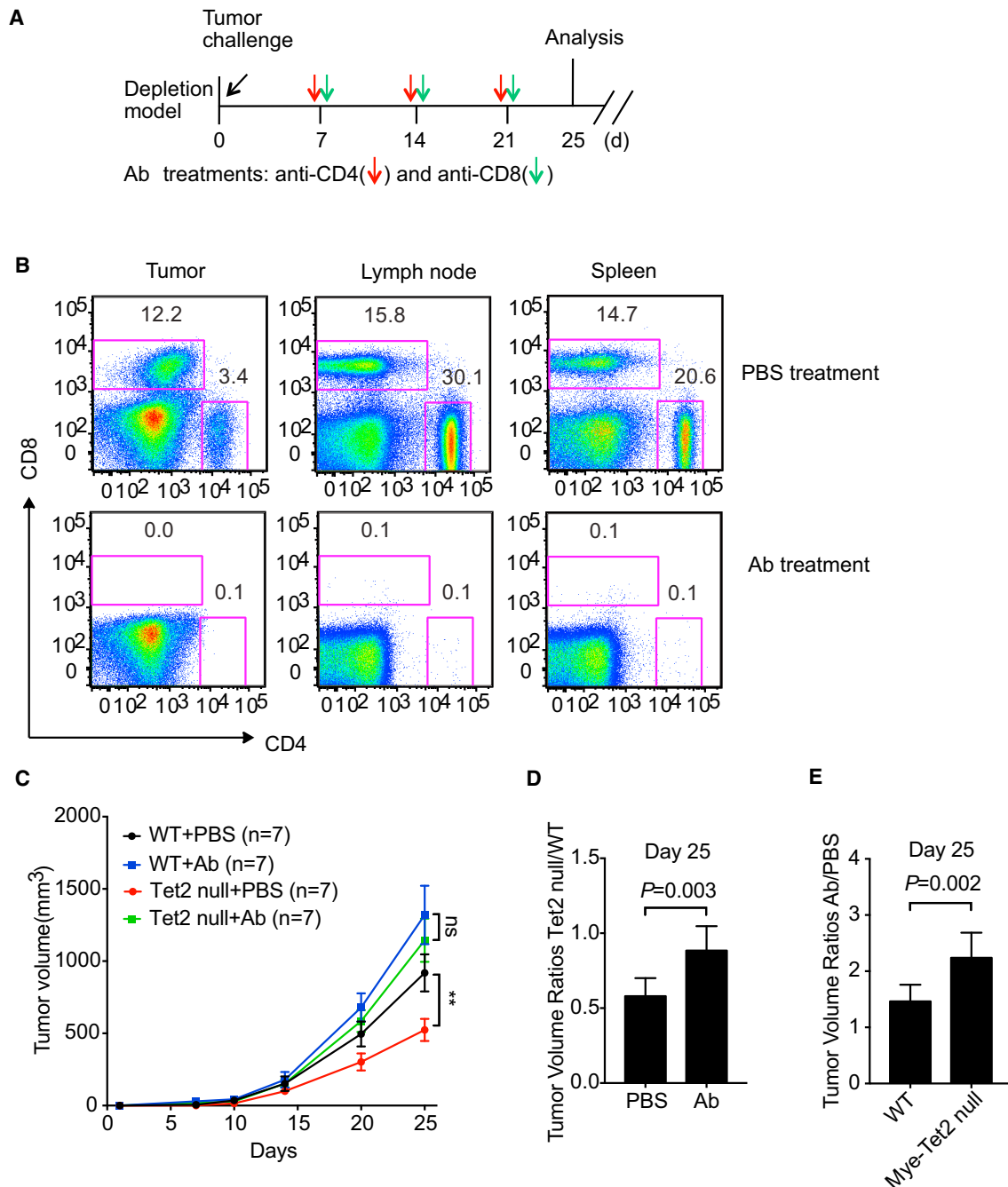


Figure 6. T Cell Depletion Abolishes the Reduced Tumor Size Phenotype Seen in Mye-Tet2-Null Mice

(A) Schematic illustration of the T cell depletion experiment. YUMM1.7 melanoma cells were injected into WT or Mye-Tet2-null mice. Anti-CD4 and anti-CD8 antibodies (Ab) were intraperitoneally injected every 7 days at the indicated time points. PBS was injected as a mock control.

(B) T cell depletion efficiencies in spleen, lymph node, and tumor were determined after three antibody injections. Representative flow cytometry plots are shown.

(C) Tumor growth curves in WT and Mye-Tet2-null mice either treated with PBS or with antibodies are shown. $n = 7$. ** $p < 0.01$; ns, not significant. Error bars represent SEM.

(D) Statistical analysis of tumor volume ratio between Mye-Tet2-null and WT mice at day 25, for PBS or Ab treatment groups.

(E) Statistical analyses of tumor volume ratio between Ab and PBS treatment groups at day 25, for WT and Mye-Tet2-null groups.

Error bars for (D) and (E) represent SD. See [STAR Methods](#) for p value determination. Data represent three (B) and two (C–E) independent experiments. Please also see [Figure S6](#).

expression in macrophages and control antiviral responses (Li et al., 2016; Xue et al., 2016). *DNMT3A* is also frequently mutated in HSCs, whose ablation leads to HSC expansion and inhibition of differentiation (Cullen and Goodell, 2015). Although *TET3* is not a major target of genetic mutations in human, murine studies have revealed that combined *Tet2* and *Tet3* ablation leads to accelerated development of a myeloid malignancy (An et al., 2015), suggesting functional cooperation between *Tet2* and *Tet3*. Further mechanistic studies in this area may lead to new avenues of clinical intervention.

STAR★METHODS

Detailed methods are provided in the online version of this paper and include the following:

- KEY RESOURCES TABLE
- CONTACT FOR REAGENT AND RESOURCE SHARING
- EXPERIMENTAL MODEL AND SUBJECT DETAILS
 - Mice
 - Human samples
 - Cell lines
- METHOD DETAILS
 - Murine tumor models and tumor harvest
 - Isolation of human melanoma CD11b⁺ cells from surgical tissues
 - Cell and tissue collection, and FACS analysis
 - Differentiation and treatment of BMDMs
 - RNA-Seq and data analysis
 - Quantitative RT-PCR
 - 5hmC DIP
 - *In vitro* T cell activation assay
 - Arginase and ROS assays
 - T cell depletion and IL-1R acute inhibition
- QUANTIFICATION AND STATISTICAL ANALYSIS
- DATA AND SOFTWARE AVAILABILITY

SUPPLEMENTAL INFORMATION

Supplemental Information includes six figures and two tables and can be found with this article online at <http://dx.doi.org/10.1016/j.immuni.2017.07.020>.

AUTHOR CONTRIBUTIONS

W.P. designed and conducted most of the experiments. S.Z., K.M., J.C., K.H., H.M., Z.W., C.R., J. Liu, Z.T., J.Z., and B.G. participated in the experiments. K.Q., J.Z., W.P., and J. Lu performed bioinformatics analysis. Y.L. and X.W. collected and analyzed human samples. M.B., R.A.F., and S.A.K. assisted with reagents, experimental design, and data interpretation. J. Lu supervised the study. J. Lu and W.P. wrote the manuscript.

ACKNOWLEDGMENTS

We thank Susan Kaech, Carla Rothlin, Shangqin Guo, Tae Kon Kim, Yi Yang, and Anna Baccei for helpful discussions, technical expertise, or critical review of this manuscript. We thank Mei Zhong from Yale Stem Cell Center Genomics Core for assistance with deep sequencing, which was supported by the Connecticut Regenerative Medicine Research Fund (RMRF) and the Li Ka Shing Foundation. We thank the assistance from the cores of Yale Cooperative Center of Excellence in Hematology. This work is supported in part by NIH grant R01CA149109 (to J. Lu), Connecticut RMRF grant

15-RMB-YALE-06 (to J. Lu), DoD grant 0011014192 (to J. Lu), a Developmental Research Award from Yale SPORE in Skin Cancer (to J. Lu), Leukemia and Lymphoma Society Fellowship No. 5338-15 (to W.P.), a fellowship from Helen Hay Whitney Foundation-Howard Hughes Medical Institute (to S.Z.), and a grant from the Strategic Priority Research Program of the Chinese Academy of Sciences No. XDPB03 (to S.Z.).

Received: November 28, 2016

Revised: April 29, 2017

Accepted: May 30, 2017

Published: August 15, 2017

REFERENCES

- Abram, C.L., Roberge, G.L., Hu, Y., and Lowell, C.A. (2014). Comparative analysis of the efficiency and specificity of myeloid-Cre deleting strains using ROSA-EYFP reporter mice. *J. Immunol. Methods* **408**, 89–100.
- Amit, I., Winter, D.R., and Jung, S. (2016). The role of the local environment and epigenetics in shaping macrophage identity and their effect on tissue homeostasis. *Nat. Immunol.* **17**, 18–25.
- An, J., González-Avalos, E., Chawla, A., Jeong, M., López-Moyado, I.F., Li, W., Goodell, M.A., Chavez, L., Ko, M., and Rao, A. (2015). Acute loss of TET function results in aggressive myeloid cancer in mice. *Nat. Commun.* **6**, 10071.
- Bhatia, S., and Thompson, J.A. (2014). Melanoma: immune checkpoint blockade story gets better. *Lancet* **384**, 1078–1079.
- Biswas, S.K., Sica, A., and Lewis, C.E. (2008). Plasticity of macrophage function during tumor progression: regulation by distinct molecular mechanisms. *J. Immunol.* **180**, 2011–2017.
- Busque, L., Patel, J.P., Figueroa, M.E., Vasanthakumar, A., Provost, S., Hamilou, Z., Mollica, L., Li, J., Viale, A., Heguy, A., et al. (2012). Recurrent somatic TET2 mutations in normal elderly individuals with clonal hematopoiesis. *Nat. Genet.* **44**, 1179–1181.
- Callahan, M.K. (2016). Immune checkpoint therapy in melanoma. *Cancer J.* **22**, 73–80.
- Carmi, Y., Voronov, E., Dotan, S., Lahat, N., Rahat, M.A., Fogel, M., Huszar, M., White, M.R., Dinarello, C.A., and Apte, R.N. (2009). The role of macrophage-derived IL-1 in induction and maintenance of angiogenesis. *J. Immunol.* **183**, 4705–4714.
- Cataisson, C., Salcedo, R., Hakim, S., Moffitt, B.A., Wright, L., Yi, M., Stephens, R., Dai, R.M., Lyakh, L., Schenten, D., et al. (2012). IL-1R-MyD88 signaling in keratinocyte transformation and carcinogenesis. *J. Exp. Med.* **209**, 1689–1702.
- Chen, Q., Chen, Y., Bian, C., Fujiki, R., and Yu, X. (2013). TET2 promotes histone O-GlcNAcylation during gene transcription. *Nature* **493**, 561–564.
- Chin, L. (2003). The genetics of malignant melanoma: lessons from mouse and man. *Nat. Rev. Cancer* **3**, 559–570.
- Church, S.E., and Galon, J. (2015). Tumor microenvironment and immunotherapy: the whole picture is better than a glimpse. *Immunity* **43**, 631–633.
- Colegio, O.R., Chu, N.Q., Szabo, A.L., Chu, T., Rhebergen, A.M., Jairam, V., Cyrus, N., Brokowski, C.E., Eisenbarth, S.C., Phillips, G.M., et al. (2014). Functional polarization of tumour-associated macrophages by tumour-derived lactic acid. *Nature* **513**, 559–563.
- Cullen, S.M., and Goodell, M.A. (2015). Dynamic DNA methylation discovered during HSC differentiation. *Cell Cycle* **14**, 693–694.
- Dankort, D., Curley, D.P., Cartlidge, R.A., Nelson, B., Karnezis, A.N., Damsky, W.E., Jr., You, M.J., DePinho, R.A., McMahon, M., and Bosenberg, M. (2009). Braf(V600E) cooperates with Pten loss to induce metastatic melanoma. *Nat. Genet.* **41**, 544–552.
- Davies, H., Bignell, G.R., Cox, C., Stephens, P., Edkins, S., Clegg, S., Teague, J., Woffendin, H., Garnett, M.J., Bottomley, W., et al. (2002). Mutations of the BRAF gene in human cancer. *Nature* **417**, 949–954.
- Delhommeau, F., Dupont, S., Della Valle, V., James, C., Trannoy, S., Massé, A., Kosmider, O., Le Couedic, J.P., Robert, F., Alberdi, A., et al. (2009). Mutation in TET2 in myeloid cancers. *N. Engl. J. Med.* **360**, 2289–2301.

- Doedens, A.L., Stockmann, C., Rubinstein, M.P., Liao, D., Zhang, N., DeNardo, D.G., Coussens, L.M., Karin, M., Goldrath, A.W., and Johnson, R.S. (2010). Macrophage expression of hypoxia-inducible factor-1 alpha suppresses T-cell function and promotes tumor progression. *Cancer Res.* **70**, 7465–7475.
- Figueroa, M.E., Abdel-Wahab, O., Lu, C., Ward, P.S., Patel, J., Shih, A., Li, Y., Bhagwat, N., Vasanthakumar, A., Fernandez, H.F., et al. (2010). Leukemic IDH1 and IDH2 mutations result in a hypermethylation phenotype, disrupt TET2 function, and impair hematopoietic differentiation. *Cancer Cell* **18**, 553–567.
- Franklin, R.A., Liao, W., Sarkar, A., Kim, M.V., Bivona, M.R., Liu, K., Pamer, E.G., and Li, M.O. (2014). The cellular and molecular origin of tumor-associated macrophages. *Science* **344**, 921–925.
- Genovese, G., Kähler, A.K., Handsaker, R.E., Lindberg, J., Rose, S.A., Bakhoum, S.F., Chambert, K., Mick, E., Neale, B.M., Fromer, M., et al. (2014). Clonal hematopoiesis and blood-cancer risk inferred from blood DNA sequence. *N. Engl. J. Med.* **371**, 2477–2487.
- He, Y.F., Li, B.Z., Li, Z., Liu, P., Wang, Y., Tang, Q., Ding, J., Jia, Y., Chen, Z., Li, L., et al. (2011). Tet-mediated formation of 5-carboxylcytosine and its excision by TDG in mammalian DNA. *Science* **333**, 1303–1307.
- Ho, P.C., Bihuniak, J.D., Macintyre, A.N., Staron, M., Liu, X., Amezcua, R., Tsui, Y.C., Cui, G., Micevic, G., Perales, J.C., et al. (2015). Phosphoenolpyruvate is a metabolic checkpoint of anti-tumor T cell responses. *Cell* **162**, 1217–1228.
- Huang, Y., and Rao, A. (2014). Connections between TET proteins and aberrant DNA modification in cancer. *Trends Genet.* **30**, 464–474.
- Ichihama, K., Chen, T., Wang, X., Yan, X., Kim, B.S., Tanaka, S., Ndiaye-Lobry, D., Deng, Y., Zou, Y., Zheng, P., et al. (2015). The methylcytosine dioxygenase Tet2 promotes DNA demethylation and activation of cytokine gene expression in T cells. *Immunity* **42**, 613–626.
- Ito, S., Shen, L., Dai, Q., Wu, S.C., Collins, L.B., Swenberg, J.A., He, C., and Zhang, Y. (2011). Tet proteins can convert 5-methylcytosine to 5-formylcytosine and 5-carboxylcytosine. *Science* **333**, 1300–1303.
- Jablonski, K.A., Amici, S.A., Webb, L.M., Ruiz-Rosado, Jde.D., Popovich, P.G., Partida-Sanchez, S., and Guerau-de-Arellano, M. (2015). Novel markers to delineate murine M1 and M2 macrophages. *PLoS ONE* **10**, e0145342.
- Jaiswal, S., Fontanillas, P., Flannick, J., Manning, A., Grauman, P.V., Mar, B.G., Lindsley, R.C., Mermel, C.H., Burt, N., Chavez, A., et al. (2014). Age-related clonal hematopoiesis associated with adverse outcomes. *N. Engl. J. Med.* **371**, 2488–2498.
- Ko, M., Huang, Y., Jankowska, A.M., Pape, U.J., Tahiliani, M., Bandukwala, H.S., An, J., Lamperti, E.D., and Guerau-de-Arellano, M. (2010). Impaired hydroxylation of 5-methylcytosine in myeloid cancers with mutant TET2. *Nature* **468**, 839–843.
- Ko, M., Bandukwala, H.S., An, J., Lamperti, E.D., Thompson, E.C., Hastie, R., Tsangaratos, A., Rajewsky, K., Korolov, S.B., and Rao, A. (2011). Ten-Eleven-Translocation 2 (TET2) negatively regulates homeostasis and differentiation of hematopoietic stem cells in mice. *Proc. Natl. Acad. Sci. USA* **108**, 14566–14571.
- Langemeijer, S.M., Kuiper, R.P., Berends, M., Knops, R., Aslanyan, M.G., Massop, M., Stevens-Linders, E., van Hoogen, P., van Kessel, A.G., Raymakers, R.A., et al. (2009). Acquired mutations in TET2 are common in myelodysplastic syndromes. *Nat. Genet.* **41**, 838–842.
- Lewis, A.M., Varghese, S., Xu, H., and Alexander, H.R. (2006). Interleukin-1 and cancer progression: the emerging role of interleukin-1 receptor antagonist as a novel therapeutic agent in cancer treatment. *J. Transl. Med.* **4**, 48.
- Li, Z., Cai, X., Cai, C.L., Wang, J., Zhang, W., Petersen, B.E., Yang, F.C., and Xu, M. (2011). Deletion of Tet2 in mice leads to dysregulated hematopoietic stem cells and subsequent development of myeloid malignancies. *Blood* **118**, 4509–4518.
- Li, X., Zhang, Q., Ding, Y., Liu, Y., Zhao, D., Zhao, K., Shen, Q., Liu, X., Zhu, X., Li, N., et al. (2016). Methyltransferase Dnmt3a upregulates HDAC9 to deacetylate the kinase TBK1 for activation of antiviral innate immunity. *Nat. Immunol.* **17**, 806–815.
- Marvel, D., and Gabrilovich, D.I. (2015). Myeloid-derived suppressor cells in the tumor microenvironment: expect the unexpected. *J. Clin. Invest.* **125**, 3356–3364.
- Meeth, K., Wang, J.X., Micevic, G., Damsky, W., and Bosenberg, M.W. (2016). The YUMM lines: a series of congenic mouse melanoma cell lines with defined genetic alterations. *Pigment Cell Melanoma Res.* **29**, 590–597.
- Moran-Crusio, K., Reavie, L., Shih, A., Abdel-Wahab, O., Ndiaye-Lobry, D., Lobry, C., Figueroa, M.E., Vasanthakumar, A., Patel, J., Zhao, X., et al. (2011). Tet2 loss leads to increased hematopoietic stem cell self-renewal and myeloid transformation. *Cancer Cell* **20**, 11–24.
- Muzio, M., Ni, J., Feng, P., and Dixit, V.M. (1997). IRAK (Pelle) family member IRAK-2 and MyD88 as proximal mediators of IL-1 signaling. *Science* **278**, 1612–1615.
- Ngjow, S.F., Meeth, K.M., Stannard, K., Barkauskas, D.S., Bollag, G., Bosenberg, M., and Smyth, M.J. (2015). Co-inhibition of colony stimulating factor-1 receptor and BRAF oncogene in mouse models of BRAF(V600E) melanoma. *Oncol Immunology* **5**, e1089381.
- Noy, R., and Pollard, J.W. (2014). Tumor-associated macrophages: from mechanisms to therapy. *Immunity* **41**, 49–61.
- Okabe, Y., and Medzhitov, R. (2014). Tissue-specific signals control reversible program of localization and functional polarization of macrophages. *Cell* **157**, 832–844.
- Ostuni, R., Kratochvill, F., Murray, P.J., and Natoli, G. (2015). Macrophages and cancer: from mechanisms to therapeutic implications. *Trends Immunol.* **36**, 229–239.
- Pauleau, A.L., Rutschman, R., Lang, R., Pernis, A., Watowich, S.S., and Murray, P.J. (2004). Enhancer-mediated control of macrophage-specific arginase I expression. *J. Immunol.* **172**, 7565–7573.
- Pietras, E.M., Mirantes-Barbeito, C., Fong, S., Loeffler, D., Kovtonyuk, L.V., Zhang, S., Lakshminarasimhan, R., Chin, C.P., Techner, J.M., Will, B., et al. (2016). Chronic interleukin-1 exposure drives haematopoietic stem cells towards precocious myeloid differentiation at the expense of self-renewal. *Nat. Cell Biol.* **18**, 607–618.
- Qian, B.Z., and Pollard, J.W. (2010). Macrophage diversity enhances tumor progression and metastasis. *Cell* **141**, 39–51.
- Quivoron, C., Couronné, L., Della Valle, V., Lopez, C.K., Plo, I., Wagner-Ballon, O., Do Cruzeiro, M., Delhommeau, F., Arnulf, B., Stern, M.H., et al. (2011). TET2 inactivation results in pleiotropic hematopoietic abnormalities in mouse and is a recurrent event during human lymphomagenesis. *Cancer Cell* **20**, 25–38.
- Rawal, S., Park, H.J., Chu, F.L., Zhang, M., Nattamai, D., Kannan, S.C., Sharma, R., Delgado, D.A., Chou, T., Davis, R.E., and Neelapu, S.S. (2011). Role of IL-4 in inducing immunosuppressive tumor microenvironment in follicular lymphoma. *Blood* **118**, 349–350.
- Rodriguez, P.C., Hernandez, C.P., Quiceno, D., Dubinett, S.M., Zabaleta, J., Ochoa, J.B., Gilbert, J., and Ochoa, A.C. (2005). Arginase I in myeloid suppressor cells is induced by COX-2 in lung carcinoma. *J. Exp. Med.* **202**, 931–939.
- Sharda, D.R., Yu, S., Ray, M., Squadrito, M.L., De Palma, M., Wynn, T.A., Morris, S.M., Jr., and Hankey, P.A. (2011). Regulation of macrophage arginase expression and tumor growth by the Ron receptor tyrosine kinase. *J. Immunol.* **187**, 2181–2192.
- Tahiliani, M., Koh, K.P., Shen, Y., Pastor, W.A., Bandukwala, H., Brudno, Y., Agarwal, S., Iyer, L.M., Liu, D.R., Aravind, L., and Rao, A. (2009). Conversion of 5-methylcytosine to 5-hydroxymethylcytosine in mammalian DNA by MLL partner TET1. *Science* **324**, 930–935.
- Tsagaratos, A., Äijö, T., Lio, C.W., Yue, X., Huang, Y., Jacobsen, S.E., Lähdesmäki, H., and Rao, A. (2014). Dissecting the dynamic changes of 5-hydroxymethylcytosine in T-cell development and differentiation. *Proc. Natl. Acad. Sci. USA* **111**, E3306–E3315.
- Voronov, E., Shouval, D.S., Krelin, Y., Cagnano, E., Benharroch, D., Iwakura, Y., Dinarello, C.A., and Apte, R.N. (2003). IL-1 is required for tumor invasiveness and angiogenesis. *Proc. Natl. Acad. Sci. USA* **100**, 2645–2650.

- Voronov, E., Carmi, Y., and Apte, R.N. (2014). The role IL-1 in tumor-mediated angiogenesis. *Front. Physiol.* 5, 114.
- Wesche, H., Henzel, W.J., Shillinglaw, W., Li, S., and Cao, Z. (1997). MyD88: an adapter that recruits IRAK to the IL-1 receptor complex. *Immunity* 7, 837–847.
- Wu, H., and Zhang, Y. (2011). Mechanisms and functions of Tet protein-mediated 5-methylcytosine oxidation. *Genes Dev.* 25, 2436–2452.
- Xie, M., Lu, C., Wang, J., McLellan, M.D., Johnson, K.J., Wendl, M.C., McMichael, J.F., Schmidt, H.K., Yellapantula, V., Miller, C.A., et al. (2014). Age-related mutations associated with clonal hematopoietic expansion and malignancies. *Nat. Med.* 20, 1472–1478.
- Xue, S., Liu, C., Sun, X., Li, W., Zhang, C., Zhou, X., Lu, Y., Xiao, J., Li, C., Xu, X., et al. (2016). TET3 inhibits type I IFN production independent of DNA demethylation. *Cell Rep.* 16, 1096–1105.
- Yadav, M., and Delamarre, L. (2016). IMMUNOTHERAPY. Outsourcing the immune response to cancer. *Science* 352, 1275–1276.
- Yang, R., Qu, C., Zhou, Y., Konkel, J.E., Shi, S., Liu, Y., Chen, C., Liu, S., Liu, D., Chen, Y., et al. (2015). Hydrogen sulfide promotes Tet1- and Tet2-mediated Foxp3 demethylation to drive regulatory T cell differentiation and maintain immune homeostasis. *Immunity* 43, 251–263.
- Ye, M., Iwasaki, H., Laiosa, C.V., Stadtfeld, M., Xie, H., Heck, S., Clausen, B., Akashi, K., and Graf, T. (2003). Hematopoietic stem cells expressing the myeloid lysozyme gene retain long-term, multilineage repopulation potential. *Immunity* 19, 689–699.
- Zhang, Q., Zhao, K., Shen, Q., Han, Y., Gu, Y., Li, X., Zhao, D., Liu, Y., Wang, C., Zhang, X., et al. (2015). Tet2 is required to resolve inflammation by recruiting Hdac2 to specifically repress IL-6. *Nature* 525, 389–393.

STAR★METHODS

KEY RESOURCES TABLE

REAGENT or RESOURCE	SOURCE	IDENTIFIER
Antibodies		
Pacific Blue anti-mouse CD45.2 Antibody	Biolegend	Cat#109820; RRID: AB_492872
PE anti-mouse/human CD11b Antibody	Biolegend	Cat#101208; RRID: AB_312791
APC anti-mouse F4/80 Antibody	eBioscience	Cat#17-4801-82
APC/Cy7 anti-mouse Gr-1 Antibody	Biolegend	Cat#108424; RRID: AB_2137485
PE/Cy7 anti-mouse Ly-6G Antibody	Biolegend	Cat#127618; RRID: AB_1877261
APC anti-mouse Ly-6C Antibody	Biolegend	Cat#128016; RRID: AB_1732076
PE anti-mouse CD3e Antibody	Biolegend	Cat#100308; RRID: AB_312673
APC anti-mouse CD4 Antibody	Biolegend	Cat#100412; RRID: AB_312697
FITC anti-mouse CD8a Antibody	Biolegend	Cat#140404; RRID: AB_10643587
APC anti-mouse NK1.1 Antibody	Biolegend	Cat#108710; RRID: AB_313397
FITC anti-mouse Ly-6G Antibody	Biolegend	Cat#127606; RRID: AB_1236494
PE anti-mouse IFN- γ Antibody	Biolegend	Cat#505808; RRID: AB_315402
CD3e monoclonal Antibody, Functional Grade	eBioscience	Cat#16-0031-82
CD28 monoclonal Antibody, Functional Grade	eBioscience	Cat#16-0281-82
InVivoMab anti-mouse CD4	BioXCell	Cat#BE0003-1; RRID: AB_1107636
InVivoMab anti-mouse CD8a	BioXCell	Cat#BP0004-1
Foxp3 Staining Buffer Set	eBioscience	Cat#00-5523-00
5hmC antibody	Active motif	Cat#39791
CD11b microbeads	Miltenyi Biotec	Cat#130-049-601
Bacterial and Virus Strains		
DH5a competent cells	ThermoFisher	Cat#18265017
Biological Samples		
PBMC from melanoma patients	Sun Yat-Sen University affiliated Cancer Center,China	N/A
Tumor tissue from melanoma patients	Sun Yat-Sen University affiliated Cancer Center,China	N/A
Chemicals, Peptides, and Recombinant Proteins		
Recombinant Mouse M-CSF	Biolegend	Cat#576406
Recombinant human arginase I	Biolegend	Cat#552502
Recombinant Mouse IL-4	Biolegend	Cat#574306
Recombinant Mouse IL-1 β	Biolegend	Cat# 575106
Lipopolysaccharides	Sigma	Cat# L2018
Phorbol 12-myristate 13-acetate	Sigma	Cat# 16561-29-8
Ionomycin calcium salt	Sigma	Cat# I3909
Brefeldin A	Sigma	Cat# B5936
N ω -Hydroxy-nor-L-arginine	Sigma	Cat# 399275
Carboxy-H2DFFDA	Sigma	Cat# C13293
Recombinant IL-1 receptor antagonist	Biolegend	Cat#553908
Dynabeads Protein G	ThermoFisher	Cat#10003D
Human CD11b MicroBeads	Miltenyi Biotec	Cat#130-049-601
DNase I	Roche	Cat#4716728001
Collagenase IV	Worthington	Cat#CLSS-4
SuperScript III Reverse Transcriptase	Thermo Fisher	Cat#18080093
SYBR Green PCR Master Mix	Thermo Fisher	Cat# 4367659
TriZol	Thermo Fisher	Cat#15596018

(Continued on next page)

Continued

REAGENT or RESOURCE	SOURCE	IDENTIFIER
Critical Commercial Assays		
Arginase activity assay kit	Sigma	Cat# MAK112
NEBNext DNA Library Prep Master Mix Set for Illumina	NEB	Cat# E6040
NEBNext Multiplex Oligos for Illumina preparation kit	NEB	Cat# E7335
CellTrace CFSE Cell Proliferation Kit	Thermo Fisher	Cat# C34554
EasySep Mouse CD4+ T Cell Isolation Kit	StemCell Technologies	Cat#19752
EasySep Mouse CD11b Positive Selection Kit II	StemCell Technologies	Cat#18970
Deposited Data		
RNA seq analysis of BMDM under M0 and M2 condition	This paper	GSE98964
RNA seq analysis of TAMs from tumor-bearing mice	This paper	GSE98964
5hmc DIP analysis of BMDMs under M0 and M2 condition	This paper	GSE98964
Experimental Models: Cell Lines		
Braf ^{v600E} Pten ^{-/-} Cdkn2a ^{-/-} mouse melanoma cell line	Marcus W.Bosenburg, Yale University	N/A
B16-OVA	Richard A. Flavell, Yale University	N/A
Raw264.7	Richard A. Flavell, Yale University	N/A
Experimental Models: Organisms/Strains		
C57BL/6J mice	The Jackson Lab	stock#000664; RRID: IMSR_JAX:000664
Lysm ^{cre/wt}	The Jackson Lab	stock#004781; RRID: IMSR_JAX:004781
Tet2 ^{fl/fl}	The Jackson Lab	stock#017573; RRID: IMSR_JAX:017573
Tet2 ^{-/-}	The Jackson Lab	stock#023359; RRID: IMSR_JAX:023359
Myd88 ^{-/-}	The Jackson Lab	stock#009088; RRID: IMSR_JAX:009088
Il1r1 ^{-/-}	The Jackson Lab	stock#003245; RRID: IMSR_JAX:003245
Oligonucleotides		
PCR primers	Integrated DNA Technologies	see Table S1
Software and Algorithms		
FlowJo v.9.3.2	FlowJo, LLC	N/A
MATLAB (2016b)	Mathworks	N/A
Other		
Fixation/Permeabilization Solution	BD Biosciences	Cat#554715
ACK lysis buffer	Thermo Fisher	Cat#A1049201
DMEM medium	Thermo Fisher	Cat#11995065
RPMI medium	Thermo Fisher	Cat#11875093
Fetal bovine serum	Thermo Fisher	Cat#16000044
Penicillin/streptomycin/glutamine	Thermo Fisher	Cat#10378016

CONTACT FOR REAGENT AND RESOURCE SHARING

Further information and requests for resources should be directed to and will be fulfilled by the Lead Contact, Jun Lu (jun.lu@yale.edu).

EXPERIMENTAL MODEL AND SUBJECT DETAILS**Mice**

All animal experiments were performed in accordance with the guidelines of Yale University's Institutional Animal Care and Use Committee and the guidelines of NIH. All mice were housed in facilities of the Yale Animal Resources Center (YARC) with husbandry

service provided by YARC. Yale University is registered as a research facility with the United States Department of Agriculture, and is fully accredited by the Association for Assessment and Accreditation of Laboratory Animal Care. In addition, an Animal Welfare Assurance is on file with OLAW-NIH. *Lysm^{cre/wt}*, *Tet2^{fl/fl}*, *Tet2^{-/-}* and C57BL/6J mice were purchased from the Jackson Laboratory. Mye-Tet2 null mice were generated by crossing *Lysm^{cre/wt}* and *Tet2^{fl/fl}* mice. Litter mate *Lysm^{wt/wt}*, *Tet2^{fl/fl}* mice were used as controls. All mice used were on a C57BL/6J background. *Myd88^{-/-}* and *Il1r1^{-/-}* mice were originated from the Jackson Laboratory. In all tumor experiments, 6–8 week old male mice were used due to YUMM1.7 cells being of male origin and the B16 tumor model having similar behavior in male and female hosts.

Human samples

All human samples were obtained with informed consent and approved by the Research Ethics Board of Sun Yat-Sen University affiliated Cancer Center. A total of six Chinese patients with melanoma were enrolled during 2017. Peripheral blood mononuclear cells were collected and enriched by density gradient centrifugation. Freshly resected melanoma tissue was dissociated and single cell suspension was obtained. CD11b⁺ myeloid cells from peripheral blood and melanoma tissue were further enriched by CD11b MicroBeads (Miltenyi Biotec).

Cell lines

YUMM1.7 melanoma cells (*Braf^{V600E}Pten^{-/-}Cdkn2a^{-/-}*) and B16-OVA cells were maintained in complete RPMI medium 1640 (Thermo Fisher), with 10% fetal bovine serum (FBS) and 1% penicillin/streptomycin/glutamine (PSG) at 37°C and 5% CO₂. Raw264.7 cells were kept in complete Dulbecco's Modified Eagle Medium (DMEM) with 10% FBS and 1% PSG at 37°C and 5% CO₂. Raw264.7 cells were gently scraped off from culture dish using a sterile scraper when passage was needed.

METHOD DETAILS

Murine tumor models and tumor harvest

YUMM1.7 melanoma cells and B16-OVA cells were injected subcutaneously into the flanks of mice (2×10^5 cells per injection in 100 μ L PBS). Male C57BL/6J mice of 6 to 8 weeks of age were used. Tumor volume was determined by measuring the length, width and height of the tumor with a caliper, and calculated by $(1/6) \times \pi \times (\text{Length} \times \text{Width} \times \text{Height})$. The mice were euthanized on indicated days in the figures. Tumors were resected and transferred to 5 mL PBS on ice. Tumor weight was measured on a scale by transferring the specimen to a sterile Petri dish after removal of surface moisture with Kimwipes. The tumors from all experiments were then processed for flow cytometry analysis or FACS-sorting on the same day. The resected mouse tumors were mechanically dissociated with surgical scissors and digested with Collagenase IV (Worthington) and DNase I (Roche) in PBS for 30min in a 37°C shaking incubator (150 rpm). After enzymatic dissociation, the samples were transferred to ice to stop the reaction. The tumor suspension was then filtered using a 70 μ m cell strainer (Becton Dickinson) and washed with the FACS buffer (0.5% FBS in PBS) and centrifuged at 1,300 rpm. at 4°C in an Eppendorf 5810R centrifuge (similar centrifugation parameters were used throughout). Red blood cells were lysed with ACK lysis buffer (Thermo Fisher) followed by washing with the FACS buffer. The samples were then resuspended in the FACS buffer. The samples were kept on ice throughout the rest of the staining procedure.

Isolation of human melanoma CD11b⁺ cells from surgical tissues

The tumor tissue was placed on ice and a scalpel was used to trim off any evident stromal, fat, and necrotic portions of the tumor. The remaining tumor tissue was then finely minced with a razor blade on a Petri dish to break up large pieces > 1–2 mm in diameter. The melanoma tissue was then dissociated in a tube containing ~10–30 mL of RPMI 1640 medium with Liberase Blendzyme (Roche) added at a final concentration of 60 μ g/ml. Dissociation was performed in a 37°C incubator on a rocking platform with constant mixing for 45–60 min. The dissociated tissue was then filtered through a 70 μ m nylon filter into a 50 mL conical tube. A 30 mL solution of PBS and 2% heat inactivated FBS was added to neutralize the dissociation enzyme. The cell suspension was centrifuged at 1500 rpm for 5 min at 4°C. The pellet was washed twice with 30 mL of PBS with 2% FBS. If the initial surgical sample contained a significant amount of red blood cells, the cells pellet was resuspended in 2 mL of ACK lysis buffer (Thermo Fisher) and incubated for 1 min on ice, followed by the addition of 30 mL of PBS with 2% FBS, and centrifuged. The cells were subjected to the isolation of CD11b⁺ cells by using CD11b MicroBeads (Miltenyi Biotec). Peripheral blood samples were similarly enriched for CD11b⁺ cells after red cell lysis. Overall, paired peripheral blood samples and tumor tissues were obtained from six melanoma patients. Examination of mRNA expression by qRT-PCR was performed in triplicates for each sample.

Cell and tissue collection, and FACS analysis

Peritoneal macrophages were collected from the peritoneal cavity of untreated mice by injecting 10 mL of PBS followed by gentle abdominal massaging. Macrophage enrichment was performed by plating cells in RPMI with 10% FBS and 1% penicillin/ streptomycin for 2 hours at 37°C and 5% CO₂. After 2 hours, non-adherent cells were removed with three PBS washes, and cells were harvested in TRIzol for RNA extraction and qPCR analysis. Bone marrow macrophages were isolated by FACS-sorting of CD11b⁺F4/80⁺ cells. Experiments were repeated twice or more times. In each experiment, cells were collected from ~7 mice for each group. qRT-PCR analysis was performed with two replicates.

For flow cytometry analysis or FACS-sorting, single cell suspension from the tumor tissue was washed with the FACS buffer and stained with the following antibodies: anti-mouse CD45.2–Pacific blue antibody (Biolegend; clone, 30-F11; used at 1:100), anti-mouse CD11b–PE antibody (Biolegend; clone, M1/70; used at 1:200), anti-F4/80–APC antibody (eBioscience; clone BM8; used at 1:100), anti-Gr1 (Biolegend; clone RB6-8C5; used at 1:100), anti-Ly-6G-PE/Cy7 (Biolegend; clone 1A8; used at 1:400), anti-Ly-6C-APC (Biolegend; clone HK1.4; used at 1:200), anti-CD3-PE (Biolegend; clone 145-2C11; used at 1:200), anti-CD4–APC (Biolegend; clone GK1.5; used at 1:100), anti-mouse CD8a-FITC (Biolegend; clone 53-6.7; used at 1:100), anti-NK1.1-APC (Biolegend; clone PK136; used at 1:100) and anti-Ly6g-FITC (Biolegend; clone 1A8; used at 1:200) at 4°C for 15 min in the dark. The samples were then washed twice and resuspended in FACS buffer for sorting. For FACS = -sorting, live cells were first selected on the basis of forward scatter (FSC) and side scatter (SSC), followed by excluding non-single-cell events with SSC-A, SSC-W and FSC-A and FSC-W. The indicated populations were selected and sorted. Cells from other tissues were similarly processed.

For intracellular cytokine staining, cells obtained from the digested tumor mass or other sources were incubated in a tissue culture incubator for five hours at 37°C with phorbol 12-myristate 13-acetate (PMA, 50 ng/ml; Sigma), ionomycin (750 ng/ml; Sigma) and brefeldin A (10 µg/ml; Sigma). Surface staining was performed as described above with anti-mouse CD4-APC (Biolegend; clone GK1.5; used at 1:100), or anti-mouse CD8a-FITC (Biolegend; clone 53-6.7; used at 1:100). After surface staining, the cells were resuspended in Fixation/Permeabilization solution (Cytotfix/Cytoperm Kit; BD Biosciences) and intracellular cytokine staining was performed according to the manufacturer's protocol with anti-mouse IFN- γ -PE (Biolegend; clone XMG1.2; used at 1:100). For Foxp3 staining, the cells were not stimulated with PMA and ionomycin; instead, they were stained according to the manufacturer's protocol (Foxp3 Staining Buffer Set, eBioscience). For all flow cytometry data, each dot represents one mouse. Experiments were repeated twice or more times. For one batch of experiments, usually more than five mice were used for each group.

Differentiation and treatment of BMDMs

Total bone marrow cells were harvested from femur bones into the FACS buffer. Cell suspension was filtered through a 70 µm nylon strainer into a 50 mL tube. ACK lysis buffer (Thermo Fisher, 5 ml) was then added to lyse the red blood cells for 2 min at room temperature. To stop the lysis reaction, 20 mL RPMI with 2% FBS was added and the tube was centrifuged at 1500 rpm for 5 min at 4°C. The cell pellet was washed and resuspended in BMDM medium (30% L929-conditioned medium, 20% FBS, 10 ng/ml recombinant murine M-CSF (Biolegend, cat#576402) in RPMI 1640 medium, with 1% penicillin/streptomycin/glutamine). The cells were then plated at 2.5×10^6 cells per well in a sterile six-well tissue culture plate, and cultured for 7 days. To activate BMDM cells, BMDM medium was changed into DMEM medium (DMEM, 10% FBS, 1% PSG) the night before the stimulation. For IL-1 β activation, 100 ng/ml IL-1 β was added; for M2 activation, 20 ng/ml IL4 was added. The cells were then harvested at the indicated time points, and used in subsequent experiments. Two to three independent experiments were performed, with each containing three biological replicates or more (except for the RNA-seq samples with two replicates). qRT-PCR analysis was performed with two replicates for each sample.

RNA-Seq and data analysis

RNA-Seq library preparation and sequencing for BMDM samples were performed by Yale Center for Genomic Analysis, through ribosomal RNA depletion. Sequencing was performed on an Illumina 2500 machine. RNA-Seq library preparation and sequencing for TAM samples were conducted at Yale Stem Cell Center Genomics Core facility through poly A enrichment (Illumina TruSeq Stranded mRNA Library Prep Kit). RNA-Seq fastq files were processed in the GenePattern package, by first performing TopHat alignment to the mm9 mouse genome assembly, followed by quantification by CuffDiff. The resultant fpkm data were analyzed with custom MATLAB codes. For BMDM data, differentially expressed genes were identified by ANOVA analysis between the experimental groups and time points, and further filtered for at least 1.5 fold changes. Pathway analysis was performed using DAVID and Ingenuity Pathway Analysis. For TAM data, differentially expressed genes were identified by satisfying both Student's t test nominal p value of less than 0.05 and having mean log₂ expression difference of at least 1. For analysis of M1 and M2 signatures, gene set enrichment analysis (GSEA) was performed by using the Broad Institute's GSEA program, using custom gene sets. Two independent sets of signatures were used (Table S2). M1 Signature 1 and M2 Signature 1 were derived ourselves by comparing transcriptomic data of M1 (LPS treated) and M2 (IL4 treated) BMDMs treated for 10 hours and 24 hours versus those from M0 BMDMs (not treated). M1 Signature 2 and M2 Signature 2 were copied from M1 distinct gene set and M2 distinct gene set in Jablonski et al. (Jablonski et al., 2015) with duplicate gene symbols removed. Our own M1 and M2 signatures were derived as follows. For either M1 or M2, treatment data were compared to untreated cells (M0) at 10 hour and 24 hours. Signature genes satisfied the following criteria: mean log₂ fpkm expression of treated samples is more than 2; mean log₂ expression of treated samples minus the mean log₂ expression of M0 samples is more than log₂(5); mean log₂ expression of opposite polarization at 10 hour minus mean log₂ expression of M0 samples is less than 0.2; signature genes satisfying the above criteria at either 10 hours or 24 hours of treatment.

Quantitative RT-PCR

Total RNA was extracted from the cells and mouse tissues with TRIzol reagent (Thermo Fisher) according to the manufacturer's protocol. cDNA was synthesized with SuperScript III reagent kit (Thermo Fisher). The expression of the genes encoding mouse *Tet2*, *Tet3*, *Arg1*, *Mgl2*, *Iil10*, *Irf4*, and *Klf4* etc. were quantified by real-time PCR using the SYBR Green PCR Master Mix (Thermo Fisher). All gene expression results were normalized to the expression of the housekeeping gene *Rpl13a*. Amplification of cDNA was performed on an ABI Prism 7900 HT cycler (Applied Biosystems) or a Biorad CFX96 machine. Gene expression data were analyzed

by calculating the threshold values (Ct) and fold changes relative to an internal control. Primers used in this study are listed in [Table S1](#). qRT-PCR analysis of gene expression was usually performed with more than two technical replicates.

5hmC DIP

For genome-wide analysis of 5hmC distributions, 5hmC DIP analysis was performed. Library preparation was performed according to the protocols in NEBNext DNA Library Prep Master Mix Set for Illumina (NEB, E6040). Briefly, genomic DNA was sonicated to ~200bp fragments. Ten micrograms of sonicated genomic DNA were then used to ligate with the adaptor, provided in the kit, following the manufacturer's instructions. Sonicated and adaptor-ligated genomic DNA fragments were incubated with 5 μ L of 5hmC antibody (Active Motif, 39791) at 4°C overnight in a final volume of 500 μ L in DIP buffer (10 mM sodium phosphate, pH 7.0, 140 mM NaCl, 0.05% Triton X-100). The immunoprecipitated DNA fragments were enriched with Dynabeads Protein G (Thermo Fisher) and amplified with the primers provided in the NEBNext Multiplex Oligos for Illumina preparation kit (NEB, E7335). The prepared libraries were sequenced on an Illumina HiSeq2000 machine at Yale Stem Cell Center. One library was prepared for each condition indicated.

In vitro T cell activation assay

Mouse splenic CD4⁺ T cells were isolated by MACS-based purification (Stem Cell Technologies). T cells were labeled with 1 mM CFSE (Invitrogen) in pre-warmed PBS for 10 min at 37°C. The CFSE-labeled CD4⁺ T cells were then plated in complete RPMI media (with 10% FBS, 2mM glutamine, 1% penicillin/streptomycin) supplemented with 0.05 M β -mercaptoethanol in round bottom 96-well plates (2.5 \times 10⁴ cells per well). The plates were pre-coated with 1 μ g ml⁻¹ anti-CD3 (eBioscience clone 145-2C11). 5 μ g ml⁻¹ anti-CD28 (eBioscience clone 37.51) antibodies were directly added into the medium. Purified myeloid cells (TAMs or MDSCs) were added in indicated ratios and plates were incubated at 37°C and in 5% CO₂. In experiments with BMDMs, BMDM cells were cultured under M0 or M2 conditions for more than 24h, and then the culture supernatants (200 μ l) were mixed with the CFSE-labeled T cells and were added into the 96-well assay plates pre-coated with 1 μ g ml⁻¹ anti-CD3 and 5 μ g ml⁻¹ anti-CD28. After 3 days, cells were harvested and CFSE signal in the gated CD4⁺ T cells was measured by flow cytometry (LSRII Flow Cytometer, BD Biosciences). Two or more independent experiments were performed.

Arginase and ROS assays

Arginase inhibitor N^ω-Hydroxy-nor-L-arginine was obtained from Sigma (#399275), and used at 100 μ M. Recombinant human arginase 1 protein was obtained from Biolegend (#552502), and used at 1 μ g/ml. To measure Arg1 activity, the Arginase Activity Assay Kit from Sigma (# MAK112) was used following manufacturer's instructions.

For ROS assay of MDSCs, the oxidation-sensitive dye Carboxy-H2DFFDA was obtained from Sigma (#C13293). Briefly, FACS-sorted MDSC cells were incubated at 37°C in RPMI medium in the presence of 2.5 μ M DCFDA for 30 min. For induced activation, cells were simultaneously cultured, along with DCFDA, with 30ng/ml PMA. Analysis was then conducted by flow cytometry as described above. Data are representative of two independent experiments.

T cell depletion and IL-1R acute inhibition

T cell depletion was performed by intraperitoneal injection of anti-CD4 and anti-CD8 antibodies (400 μ g each for a single dose per mouse) every 7 days from day 7 post tumor cell injection. Antibodies were from BioXCell (clones GK1.5 and 53-6.72). Recombinant IL-1 receptor antagonist (IL-1Ra, anakinra) was from Biolegend (Cat#553908). IL1Ra was administered by i.v. injection at a dose of 2.5 mg/kg. Injections were performed daily for three consecutive days from day 9 after tumor cell injections. For experiments involving later time points, two additional injections were performed on day 13 and 14 after tumor cell injection. For each experiment, seven to nine mice were used for each group.

QUANTIFICATION AND STATISTICAL ANALYSIS

Student's t test (2-tailed) was applied to all analysis comparing between two groups of samples. For the T- cell depletion experiment, permutation-based tests were performed to evaluate statistical significance, using custom MATLAB codes. Specifically, we evaluated the probability to reject the null hypothesis that T cell depletion does not alter reduced tumor size phenotype in Mye-Tet2 null mice in comparison with mock treatment. This was performed by taking all possible ratios of tumor sizes between Tet2 null and WT groups (7 tumors per group, and thus 49 total possible ratios) under a specific treatment condition. The 49 ratios in T cell-depletion conditions were then compared to the 49 ratios in the mock group to derive a t test score. Permutations were then performed for 10,000 times by randomizing the labels of WT and Tet2 null assignment, and for each permutation, a t test score was derived by comparing the two sets of 49 ratios. Two-tailed p value was calculated as the probability of observing an equal or more extreme t test score in the permutation cases than the score of the original data. Similar tests were performed to reject the null hypothesis that T cell-depletion (in comparison to mock) has the same impact on Tet2 null groups as WT groups.

DATA AND SOFTWARE AVAILABILITY

Data have been deposited in Gene Expression Omnibus. The accession number for the sequencing data reported in this paper is GSE98964.